Toward Comparing Experiment and Theory for Corroborative Research on Hingeless Rotor Stability in Forward Flight

Final Technical Report Under NASA-Ames Cooperative Agreement No.NCC 2-361
(August 1, 1985 - July 31, 1987)

By G. Gaonkar

Prepared for the Aeroflightdynamics Directorate

U. S. Army Aviation Research and Technology Activity

Ames Research Centre

Moffett Field, CA 943035

FLORIDA ATLANTIC UNIVERSITY
Department of Mechanical Engineering
School of Engineering
Boca Raton, FL 33431

August 1987

Scope of NASA-Ames Cooperative Agreement No. NCC 2-361

Work under this agreement started on August 1, 1985. This final report is presented in two parts. The first part refers to correlation between prediction based on a linear theory and the U.S. Army's 7X10 ft. wind-tunnel data on flap-lag stability in hover and forward flight. The second part refers to the effects of quasisteady stall effects on the correlation. In accordance with the Cooperative Agreement Special Provision, the University and Ames personnel collaborated on performance of research, and the papers resulting from the research are co-authored. The papers are:

1) Gaonkar, G.H., McNulty, M.J. and Nagabhushanam, J., "An Experimental and Analytical Investigation of Isolated Rotor Flap-Lag Stability in Forward Flight", 11th European Rotorcraft Forum, London, England, September 10-13, 1985, Paper No. 66.

2) Nagabhushanam, J., Gaonkar, G.H., and McNulty, M.J., "An Experimental and Analytical Investigation of Stall Effects on Flag-Lag Stability in Forward Flight", 13th European Rotorcraft Forum, Arles, France, September 8-11, 1987, Paper No. 6-2-2.

ABSTRACT

For flap-lag stability of isolated rotors, experimental and analytical investigations are conducted in hover and forward flight on the adequacy of a linear quasisteady aerodynamics theory with dynamic inflow. Forward flight effects on lag regressing mode are emphasized. Accordingly, a soft inplane hingeless rotor with three blades is tested at advance ratios as high as 0.55 and at shaft angles as high as 20°. The 1.62-m model rotor is untrimmed with an essentially unrestricted tilt of the tip path plane. In combination with lag natural frequencies, collective pitch settings and flap-lag coupling parameters, the data base comprises nearly 1200 test points (damping and frequency) in forward flight and 200 test points in hover. By computerized symbolic manipulation, a linear analytical model is developed in substall to predict stability margins with mode indentification. To help explain the correlation between theory and data it also predicts substall and stall regions of the rotor disk from equilibrium values. The correlation shows both the strengths and weaknesses of the theory in substall ($|\text{angle of attack}| \leq 12°$).

NOMENCLATURE

a	Lift curve slope, rad^{-1}
c_d	Profile drag coefficient
N	Number of blades
R	Flap-lag structural coupling parameter
r	Dimensionless (1/R) radial position
t	Dimensionless time (identical with blade azimuth position of the first blade).
α	Angle of attack
α_s	Rotor shaft angle, positive nose down
μ	Advance ratio
β_o (ζ_o), β_s (ζ_s) and β_c(ζ_c)	Multiblade flapping (lag) coordinates: collective and first order cyclic flapping (lag) components
θ	Equilibrium pitch angle= $\theta_o+\theta_s\sin\psi_k+\theta_c\cos\psi_k$
$\bar{\lambda}$	Total inflow ratio = $\mu\tan\alpha_s+\bar{\nu}$
$\bar{\nu}$	Steady induced flow = $\bar{\nu}_o+\bar{\nu}_s\ r\ \sin\psi_k + \bar{\nu}_c\ r\ \cos\psi_k$
ν_o ($\bar{\nu}_o$), ν_s ($\bar{\nu}_s$) and ν_c($\bar{\nu}_c$)	Uniform, side-to-side and fore-to-aft unsteady (steady) induced flow
Ω	Rotor rotational speed in rpm
ω_ζ	Dimensionless ($1/\Omega$) uncoupled lag frequency
ψ_k	Azimuth position of the k-th blade
γ	Lock number
$(\cdot)$	d/dt
$\lvert\ \rvert$	absolute value

1. INTRODUCTION

Relatively few investigations with concomitant corroboration of test data have been conducted on isolated rotor instabilities in forward flight.[1-3] Such an investigation is particularly desirable for lag modes which are at best weakly damped and for which the state-of-the art of predicting damping levels merits considerable refinements.[4-8] Here, we study a basic aspect of that investigation --- the adequacy of a widely used quasisteady aerodynamics theory in predicting the flap-lag stability in forward flight ($0 \leq \mu \leq .55$).

We use an experimental model which closelly approaches the simple theoretical concept of a hingeless rotor as a set of a rigid articulated flap-lag blades with spring restraint. This intentionally built-in structural simplicity facilitates isolate the aerodynamic ingredients that participate in the correlation. The analytical model is based on quasisteady aerodynamics with dynamic inflow and it is directly tailored to fit the experimental model. The correlation refers to the lag regressing mode [9] which, compared to other modes, is the lowest-frequency mode and is better suited to assessing the validity of the quasisteady aerodynamics theory. Although the theory merits substantial refinements in stall ($|\alpha| > 12^{\circ}$), we have included some correlation in stall as well. Such inclusion provides an improved interpretation of the correlation between measured and predicted data.

A specific three-bladed rotor is investigated under untrim conditions[4,11] ($\theta_s=\theta_c=0$, cyclic flapping present) and it is soft in lag for forward flight test cases. However, from an intentionally simplified experimental model, the correlation makes use of a comprehensive data-base of nearly 1400 test points with respect to Ω, R, θ_0, α_s and μ and includes cases that vary from virtual zero-thrust conditions to aerodynamically demanding cases of highly stalled conditions with advance ratio μ as high as 0.55 and shaft-tilt angle α_s as high as 20°. Such a correlation should give generally applicable qualitative results on the adequacy of the linear theory when stall is not an issue and should promote further refinements.

2. EXPERIMENTAL MODEL

The model tested was a three-bladed hingeless rotor with a diameter of 1.62 m. The rotor was designed as a set of rigid, articulated blades with spring restraint and coincident flap and lag hinges. This was accomplished by the "folded back" flexure design shown in an exploded view in Fig. 1. Taking the center of the flexural elements as the effective hinge point gives a non-dimensional hinge offset of 0.11 for the design. The blades were designed to be very stiff relative to the flexures so that the first flap and lag modes involve only rigid body blade motion. The influence of the torsional degree of freedom was minimized by keeping the first torsion frequency as high as possible. In particular, the first torsion mode frequency was above 150 Hz non-rotating, insuring a rotating first torsion frequency of at least 9/rev over the entire rotor speed range tested. The rotor properties are summarized in Table 1.

The rotor had no cyclic pitch control, and collective pitch was set manually. The blade pitch could be set by changing the angle of the blade relative to the flexure at the blade-flexure attachment, giving a structural coupling value of zero, or by changing the angle of the entire blade-flexure assembly relative to the hub, giving a structural coupling value of one.

The test stand on which the rotor was mounted included a roll gimbal which could be locked out mechanically. Rotor excitation was accomplished through this gimbal by a 50 lb (222.4N) electromagnetic shaker. The stand was designed to be as stiff as possible so that the test would closely represent the case of an isolated rotor. However, the lowest frequency of the installed stand with the gimbal locked and the rotor mounted was found to be 31 Hz, somewhat lower than what was desired. The entire test stand could be pitched forward with an electric actuator to control the rotor shaft angle. The shaft angle provided the only means of controlling the rotor loads at a given collective pitch and advance ratio. A photograph of the model installed in the wind tunnel is shown in Fig. 2.

3. ANALYTICAL MODEL

The analytical model consists of an offset-hinged rigid lag-flap model with flap and lag spring restraints at the offset hinge. The spring stiffnesses of the math model are selected such that the uncoupled rotating flap and lag natural frequencies coincide with the corresponding first-mode non-rotating natural frequencies of the experimental rotor blade. The effect of the hinge offset, which is 11.1% in lag and flap, is accounted for in rotor trim and stability analyses. The rotor is untrimmed, with an essentially unrestricted tilt of the tip path plane ($\theta_s=\theta_c=0$, and cyclic flapping present).[4, 11] The

rotor angular velocity is Ω, and with time unit $1/\Omega$, the azimuth angle of the first or the reference blade represents the dimensionless time t. The distribution of flexibility between the hub including flexures and the blade (outboard of the blade location where pitch change takes place) is simulated by an elastic coupling parameter R which is also referred to as the hub rigidity parameter. Basically, R relates the rotation of the principal axes of the blade-hub system and the blade pitch θ.

The blade airfoil aerodynamics is based on linear, quasisteady theory in substall (angle of attack $|\alpha| < 12^{\circ}$) without inclusion of compressibility or other effects due to reversed and radial flow. Steady non-uniform inflow with first - harmonic distribution ($\nu = \nu_o + \nu_s r \cos\psi_k + \nu_c r \sin\psi_k$)is assumed. The airfoil nonlinear section effects are neglected.[7,8] For the math model we take a=5.73 and $c_d = 0.0079$ (NACA 23012). [7,8] The dynamic inflow effects are included from a 3x3 inflow model based on an unsteady actuator-disk theory---the Pitt Model, which has been recently verified experimentally. [5] The equations of motion including the multiblade coordinate transformation are derived from symbolic manipulation [12,13]. For the three-bladed rotor, the 15x1 state vector comprises 12 multiblade components (β_o, $\dot{\beta}_o$, β_s, $\dot{\beta}_s$, β_c, $\dot{\beta}_c$, ζ_o, $\dot{\zeta}_o$, ζ_s, $\dot{\zeta}_s$, ζ_c, $\dot{\zeta}_c$) and 3 dynamic inflow components (ν_o, ν_s, ν_c). The computational details of Floquet transition matrix, and of damping levels and Floquet eigenvectors are respectively as in references 14 and 13.

4. EXPERIMENTAL PROCEDURES

An experimental investigation of the rotor's lag stability characteristics in hover and, especially, forward flight was conducted in the Aeroflight Dynamics Directorate's 7-by-10 foot (2.1-by-3.0 m) wind tunnel. The data was collected in two tunnel entries, the first in the summer of 1982 and the second in the summer of 1983. The model's configuration and the test procedures used were the same for both tests. The only exception to this is that for the 1982 test the hover data was taken with the wind-tunnel test section doors open and the windows removed in an attempt to reduce recirculation effects. In 1983 the hover data were taken incidental to forward flight data (Ω=750 and 1000 rpms) so the windows were left in place and doors were closed. The rotor plane itself was located about 0.63 rotor diameter above the test section floor (with the shaft vertical). However the influence of recirculation and ground effect on the hover data are not significant. [15]

For each data point obtained, the blade pitch was set manually and the rotor was tracked. The rotor was then brought up to speed and wind tunnel dynamic pressure was increased to obtain the desired advance ratio while adjusting the shaft angle to keep the rotor flapping loads within limits. Once at the test condition, the roll gimbal was unlocked and the shaker was used to excite the model at the appropriate frequency. When a good level of excitation was evident in the output of the lag bending gages, the shaker was cutoff, the roll gimbal locked out, and then transient data acquisition commenced. The data itself was digitized on-line with a sample rate of 100 Hz and a total record length of 5.12 seconds. The data was then transformed to the fixed system coordinates. Spectral analysis and the moving block technique[16] were used to

determine the frequency and damping of the response. At least two data points were obtained at each test condition and the scatter between the measurements was found to be very small.

Progressing and regressing lag mode data were obtained for the hover test conditions, but above about 600rpm the progressing mode was found to be contaminated by coupling with the lower stand mode. Because all of the forward flight conditions tested were above this rotor speed, no progressing mode data were obtained. The regressing mode data should be representative of isolated blade results over the entire rotor speed range tested and appears to be of very good quality. The hover test envelopes for both the 1982 and 1983 tests are shown in Fig. 3(a) and the forward flight test envelopes are shown in Fig. 3(b). The edges of the forward flight envelopes were set by the maximum allowable rotor flapping loads.

Table 1: Measured Model Properties

Number of Blades	3
Radius	0.81 m
Chord	0.0419 m
Airfoil Section	NACA 23012
Non-dimensional Hinge Offset	0.111
Blade Inertia About Hinge	0.01695 kg-m^2
Blade Mass Center Distance from Hinge	0.188m
Blade Mass (Outboard of Hinge)	0.204 kg
Non-rotating Flap Frequency	3.09 Hz
Non-rotating Lead-lag Frequency	7.02 Hz
Average Lead-Lag Structural Damping Ratio	0.19% critical
Lock Number γ (based on a=5.73)	7.54
Lift curve slope a	5.73
Profile drag coefficient (assumed)	0.0079

5. CORRELATION OF THEORY AND DATA

We, now come to presenting the correlation between the measured and predicted data in hover and forward flight ($0 \leq \mu \leq 0.55$). If not stated otherwise, the predicted values based on a linear theory include dynamic inflow and uniform steady inflow and the measured values include both the 1982 and 1983 test points (figure 3). To facilitate an appreciation of the scope of the correlation, we begin with an overview of the data-base. As seen from figure 3, the hovering and forward flight cases refer to zero and full structural coupling (R=0 and 1)in combination with varying rotational speeds in hover ($0 \leq \Omega \leq 1000$ rpm) and with two rotational speeds (Ω=750 and 1000 rpms) in forward flight. Further, we have four values of collectives in hover(θ_o= 0°, 4°, 6° and 8°) and three values of collectives in forward flight (θ_o = 0°, 3° and 6°). Compared with hover, the data-base in forward flight is much broader in scope, since for each collective, the shaft tilt varies from 0° to 20° in combination with different advance ratios as shown in figure 3b. Thus, given the extensive scope of the data-base and the corresponding predicted values, only a small portion of the total correlation is presented for the damping levels. (Frequency-data correlation is available in reference 17.) We also emphasize how far we can isolate different ingredients that participate in the correlation. In particular, those ingredients refer to nonuniform steady inflow and unsteady or dynamic inflow. In several cases, we also refer to nonlinear airfoil drag in substall ($|\alpha| \leq 12°$) and to stall (nonlinear airfoil drag and lift, $|\alpha| > 12°$), and heuristically identify the deviation between the theory and data with such non-linear airfoil characteristics. However, it is good to reiterate the following. The nonlinear airfoil section properties including those of drag in substall are not included. Though a linear theory is used, we include

correlation even when an appreciable portion of the rotor disk ($\geq$ 10%) is in stall. That inclusion together with stall region contours provides a better understanding of the adequacy of the linear theory and also of the possible role of airfoil aerodynamic nonlinearity.

With this as a background, we take up figure 4 which shows the lag regressing mode damping versus the rotor rotational speed for four values of collectives, $\theta = 0^\circ$, 4°, 6° and 8°. For zero pitch setting, the angle of attack is very low. This fact is well reflected in the excellent correlation between theory and data except for minor discrepancies for very low rotational speeds (say, $\Omega < 300$ rpm). Those discrepancies are consistently observed for all the four cases of collectives for $\Omega < 300$ rpm, when the predicted damping level is less than the data. The reasons for this are not known. Also for $\theta_o = 4^\circ$, 6° and 8°, the correlations is generally good. However, for $\Omega > 750$ rpm, the theory deviates from the data and that deviation increases with increasing blade pitch (compare the case for $\theta_o = 4^\circ$ with that for $\theta_o = 8^\circ$). The 1.62-m model was tested in a 2.13 x 3.05 meter test section and the ratio of model height to rotor diameter was only 0.63, a relatively low value. Therefore, additional damping values were predicted with the empirical corrections for ground and recirculation effects (that is, replacing $\bar{\nu}$ by $k\bar{\nu}$, where $k<1$ for ground effect and $k>1$ for recirculation). It was found that those deviations between theory and data are not associated with ground and recirculation effects. Though our approach to capture those effects is empirical, recent experimental evidence supports this finding. [15] Thus, in summary, figure 4 shows that the data are in general agreement with the theory except for $\Omega < 300$ for all θ_o, and for $\Omega > 750$ and $\theta^\circ_o \geq 6^\circ$.

Coming to the forward flight case, we start with the damping data for the zero-collective case with Ω = 1000 rpm and R = 0, figures 5 and 6. Figure 5 shows the damping data as a function of advance ratio for discrete values of shaft tilt α_s. Figure 6 is a cross plot of the data in Figure 5, that is, damping as a function of α_s for discrete values of advance ratio μ. Thus, figure 5 together with figure 6 provides an improved picture of the correlation between theory and data for increasing values of shaft tilt α_s and advance ratio μ. Overall, figures 5 and 6 show fairly good correlation and exhibit two main features. First, compared to the correlation for high values of $\mu\alpha_s$, the correlation is much better for low values of $\mu\alpha_s$. For example, at low advance ratios ($\mu \leq 0.15$), the correlation is remarkable even quantitatively, virtually for the entire range of shaft tilt ($0 \geq \alpha_s \leq 20^\circ$). So is the case for low values of shaft tilt ($\alpha_s \leq 4^\circ$) and for advance ratios as high as 0.55, see figure 5 for $\alpha_s = 4^\circ$. In fact, right up to the high advance ratio case of 0.3, the correlation is equally remarkable for $\alpha_s \leq 8^\circ$. For μ=0.4 and $\alpha_s \leq 4^\circ$ (figure 6), the correlation is satisfactory although the theory slightly underpredicts damping and the reasons for these minor discrepancies of underprediction are not known. That the theory shows remarkable agreement with the data for low values of $\mu\alpha_s$ is to be expected. After all, the pitch setting is zero and therefore the angle of attack is very low for low values of $\mu\alpha_s$. Coming to the second feature, we observe that with increasing μ and α_s, the theory consistently overpredicts damping and increasingly deviates from the data. For example see figure 6 for μ=0.3 and $\alpha_s > 10^\circ$ and for μ=0.4 and $\alpha_s > 6^\circ$. This is also to be expected, because the angle of attack is found to increase rapidly with increasing values of $\mu\tan\alpha_s$.

The preceding correlation for zero pitch setting shows that the discrepancy between theory and data increase with increasing values of $\mu\tan\alpha_s$. To facilitate explain this discrepancy, we refer to the stall regions of the rotor disk based on equilibrium values and use the percent stall area of the rotor disk as an objective measure of the stall effects on the theory. Figures 7a and 7b show two typical stall region ($|\alpha|<12°$) contours for μ=0.3 and 0.5. We also observe in passing that for μ=0.2 and $\alpha_s \leq 20°$, the stall region (not shown) is about 12% of the rotor disk.[17] This observation corroborates the fact that the theory exhibited good agreement with the data for μ=0.1 and 0.2 in figure 6. As seen from figures 7a and 7b more than 20% of the rotor disk is in stall for μ=0.3 and α_s=16° and for μ=0.5 and α_s=8°. It is also seen that slightly more than 10% of the rotor disk is in stall for μ=0.3 and α_s=12° (figure 7a), for μ=0.4 and α_s=6° (reference 17) and for μ=0.5 and α_s=4° (figure 7b). Since the blade has zero pitch setting, the area of the stall region increases rapidly with increasing values of μ and α_s, and at the low test Reynolds number (≈170,000) the effects of airfoil aerodynamic nonlinearity seem to become more pronounced. Therefore, with increasing values of μ and α_s, those effects seem to mask the predicted data increasingly and account for the increasing deviation between theory and data, and further, the prediction becomes increasingly suspect. A similar situation exists for the second set of data for 3° collective, taken up next.

While figure 8 refers to zero flap-lag coupling with Ω=1000 rpm, figure 9 refers to full flap-lag coupling with Ω=750 rpm. Both figures essentially show the same feature. That is, the correlation is qualitatively accurate only for low values of μ and α_s. By comparison, the correlation becomes qualitatively inaccurate with increasing values of μ and α_s, the data showing decreasing

damping and the theory predicting the opposite trend of increasing damping. To fill in details, we consider figure 8. For μ=0.2, even for $\alpha_s = 20^\circ$, the stall contour results (not shown) show that not more than 10% of the rotor disk experiences stall.[17] Thus, stall is not an issue for $\mu \leq 0.2$. However, it is seen that there is consistent difference between the theory and data. For example at μ=0.05 in figure 8, the theory under predicts damping for all values of α_s. This is possibly due to nonlinear drag in substall at the low test Reynolds number. Figures 7c and 7d also show that an appreciable portion of the rotor disk experiences stall. For example, for μ=0.3 and α_s=14°, nearly 10% of the rotor disk is in stall and the stall region for μ=0.4 rapidly increases for $\alpha_s > 8^\circ$. Thus in summary, nonlinear air foil section characteristics seem to be contributing to the discrepancies between theory and data in figures 8 and 9.

With figure 10 and 11, we come to the data-base for $\theta^\circ = 6^\circ$ and $\mu < 0.2$, also see figure 3b. The data are limited to low advance ratios and stall is not an issue here. For the complete range of shaft tilt ($0 \leq \alpha_s{}^\circ \leq 20$), the data are available only for $\mu = 0.05$. The corresponding correlation is given in figures 11a (R=0) and 11b (R=1). It is seen that the overall prediction is not satisfactory. In fact, for α_s=20° ($0 \leq \mu \leq 0.15$) the prediction shows that damping trend increases with increasing μ, a trend that is not supported by the data. This feature is quite similar to the one referred to earlier in figures 8 and 9 for $\alpha_s > 8^\circ$. Given the appreciable deviations between the theory and data for the hovering case with comparable pitch setting at Ω=1000 (e.g. figure 4 at θ°=6°), the deviations in figures 10 and 11 for μ=0.05 are not unexpected. Inspite of the appreciable underprediction, the data supports the theory in showing that the damping level virtually remains constant for the entire range of shaft tilt at μ=0.05.

We mentioned earlier that the preceding prediction includes uniform steady inflow and dynamic inflow. The final set of correlation as presented in figures 11, 12 and 13, is used to isolate the effects of nonuniform steady inflow and dynamic inflow. In figure 11, the predictions from the linear theory are shown by full lines. The predictions from that theory refined to include nonuniform steady inflow and the predictions from that theory without dynamic inflow are respectively shown by broken lines with dots and by broken lines. It is seen that nonuniform steady inflow hardly influences correlation. By comparison, dynamic inflow improves correlation throughout, but not significantly. Compared to the case with R = 1, when the improvement is at best marginal, the improvement is much better for the case with R = 0. As for dynamic inflow, we further explore its effects in figure 12 for the hovering case, and in figure 13 for the forward flight case at high advance ratios of 0.3 and 0.45. Figure 12 is a partial reproduction of figure 4 for θ_o = 6° and 8°. The improvement due to including dynamic inflow is noteworthy. However, for Ω>800 rpm, the increasing discrepancy between theory and data, particularly with increasing pitch setting, remains virtually unaffected, even with inclusion of dynamic inflow. The correlations in figures 11 and 12 do demonstrate that it is highly desirable to include dynamic inflow in predicting inplane damping. The correlation in figure 13 based on the 1982 data is extremely interesting. Here we have θ_o=0°, Ω=1000 rpm and R=0 at high advance ratios of 0.3 and 0.45. As seen from figures 7a and 7b, we should expect appreciable stall effects for α_s>10° at μ=0.30, and for α_s>4° at μ=0.45, to render the theory suspect. Two features are worth mentioning. First, in substall the improvement due to dynamic inflow is negligible for μ=0.3. For μ=0.45 and α_s<4°, when the linear theory is reasonably valid, the differences in the predicted values without and with dynamic inflow

are too small to isolate dynamic inflow effects. Second, the predicted data (without inflow), which also does not account for stall shows "better correlation" for the entire range of shaft tilt. However, stall effects increase with increasing values of μ and α_s and mask the prediction without and with dynamic inflow. The prediction in figure 13 needs to be resolved for the effects of airfoil aerodynamic nonlinearity for a valid treatment of isolating dynamic inflow effects.

6. CONCLUDING REMARKS

Thus far, we presented the correlation between theory and data on the lag regressing mode damping levels. That correlation leads to the following remarks:

1. In hover, the predictions are in general agreement with the data. However, some discrepancies at high rotational speeds and blade pitch settings are identified.
2. In forward flight at $\theta_0=0^\circ$ and 3°, the correlation is fairly good when not more than about 10% of the rotor disk is in stall. When an appreciable portion of the rotor disk is in stall (say 10% or more), the theory is at best qualitatively accurate for $\theta_0=0^\circ$, in that the theory and data show the same trend of increasing damping with increasing α_s and μ, though there is appreciable quantitative discrepancy. However, this qualitative accuracy is suspect since the nonlinear airfoil characteristics are expected to mask

the prediction increasingly with increasing values of μ and α_s. For $\theta_o=3^\circ$, the theory and data respectively show the opposite trends of increasing and decreasing damping levels with increasing α_s and μ.

3. In forward flight at $\theta_o=6^\circ$, the data are limited to low advance ratios ($\mu < 0.20$) and virtually the entire rotor disk is in substall. Still, the theory significantly deviates from the data. In fact, for $\alpha_s=20$, the prediction shows appreciably increasing damping with increasing μ, whereas the data shows slowly decreasing damping with increasing μ. For $\mu=0.05$, the data confirm the prediction that the damping level essentially remains constant for the entire range of shaft tilt ($0 \leq \alpha_s \leq 20^\circ$), and the discrepancies between the data and prediction are of the same order of magnitude as those in hover for $\theta_o=6^\circ$ and $\Omega \geq 750$ rpm.

4. Effects of nonuniform steady inflow hardly affect the predictions.

5. The inclusion of dynamic inflow consistently improves correlation appreciably in hover and marginally in forward flight. However, at high advance ratios, cases are identified for which predictions without and with dynamic inflow are masked by the effects of airfoil aerodynamic nonlinearity to pass a judgement on dynamic inflow effects.

7. ACKNOWLEDGEMENT

We are grateful to Messrs. Robert Ormiston and William Bousman for their encouragement and extensive comments. We also thank Mrs. Antonia Margetis and Mrs. Nancy Ward Anderson for their hard work and persistence in word processing this paper. This work is sponsored by the U. S. Army Aeroflight dynamics Directorate, NASA-Ames Research Center and administered under Grant NCC 2-361.

8. REFERENCES

1. Ormiston, R. A., " Investigations of Hingeless Rotor Stability", Vertica, Vol. 7, No. 2, 1983, pp. 143-181.

2. Friedmann, P. P., "Formulation and Solution of Rotary-Wing Aeroelastic Stability and Response Problems", Vertica, Vol. 7, No.2, pp.101-141, 1983.

3. Bousman, William G., "A Comparison of Theory and Experiment for Coupled Rotor-Body Stability of a Hingless Rotor" ITR Methodology Assessment Workshop, NASA Ames Research Center, Moffett Field, California, June 1983.

4. Nagabhushanam, J. and Gaonkar, G. H., "Rotorcraft Air Resonance in Forward Flight with Various Dynamic Inflow Models and Aeroelastic Couplings", Vertica, Vol.8, No. 4, December, 1984, pp. 373-394.

5. Gaonkar, G. H. and Peters, D. A., "A Review of Dynamic Inflow and Its Effect on Experimental Correlations" Proceedings of the Second Decennial Meeting on Rotorcraft Dynamics, AHS and NASA Ames Research Center, Moffett Field, California, November 7-9, 1984. Paper No. 13.

6. Neelakantan, G. R. and Gaonkar, G. H., "Feasibility of Simplifying Coupled Lag-Flap-Torsional Models For Rotor Blade Stability in Forward Flight", Vertica, Vol. 9, No.3, pp. 241 - 256.

7. Bousman, W. G., Sharpe, D. L., and Ormiston,, R. A., "An Experimental Study of Techniques for Increasing the Lead-Lag Damping of Soft Inplane Hingeless Rotors", Proceedings of the American Helicopter Society 32nd Annual National Forum, Washington, D. C., May 1976, Preprint No. 730.

8. Ormiston, R. A. and Bousman, W. G., "A Study of Stall-Induced Flap-Lag Instability of Hingeless Rotors", Preceedings of the American Helicopter Society 29th Annual National Forum, Washington, D. C., May 1973, Preprint No. 730.

9. Peters, D. A., and Gaonkar, G. H., "Theoretical Flap-Lag Damping with Various Dynamic Inflow Models," Journal of the American Helicopter Society, July 1980, Vol. 25, No. 3, pp.29-36.

10. Gaonkar, G. H. et al, "The Use of Actuator-Disc Dynamic Inflow for Helicopter Flap-Lag Stability", Journal of the American Helicopter Society, July 1983, Vol. 28, No. 3, pp 79-88.

11. Gaonkar, G. H., and Peters, D. A., "Use of Multiblade Coordinates for Helicopter Flap-Lag Stability with Dynamic Inflow," Journal of Aircraft, Vol. 17, No. 2, 1980, pp.112-118.

12. Nagabhushanam, J., Gaonkar, G. H., and Reddy, T.S.R., "Automatic Generation of Equations for Rotor-Body Systems with dynamic Inflow for A-Priori Ordering Schemes," Seventh European Rotorcraft Forum, Garmisch-Partenkirchen, Federal Republic of Germany, September 8-11, 1981, Paper No. 37

13. Nagabhushanam, J., Gaonkar, G. H., Srinivasan, P., and Reddy T.S.R., Users' Manual for Automatic Generation of Equations of Motion and Damping Levels for Some Problems of Rotorcraft Flight Dynamics, R & D Report, HAL-IISC Helicopter Program, Indian Institute of Science, Bangalore, India, October 1984.

14. Gaonkar, G. H., Simha Prasad, D. S., and Sastry, D. S. "On Computing Floquet Transition Matrices of Rotorcraft", Journal of the American Helicopter Society, Vol. 26, No. 3, July 1981, pp. 56-62.

15. Sharpe, D. L., An Experimental Investigation of the Flap-Lag-Torsion Aeroelastic Stability of a Small-Scale Hingeless Helicopter Rotor in Hover, AVSCOM-TR-89-A-9, January 1986.

16. Bousman, W.G., and Winkler, D.J. "Application of the Moving-Block Analysis" 22nd Structures, Structural Dynamics, and Materials Conference, Atlanta, Ga. April 1981. Paper 81-0653-CP.

17. Gaonkar, G. H., McNulty, M. J. and Nagabhushanam, J., "An Experimental and Analytical Investigation of Isolated Rotor Flap-Lag Stability in Forward Flight," Eleventh European Rotorcraft Forum, London, England, September 10-13, 1985, paper No. 66.

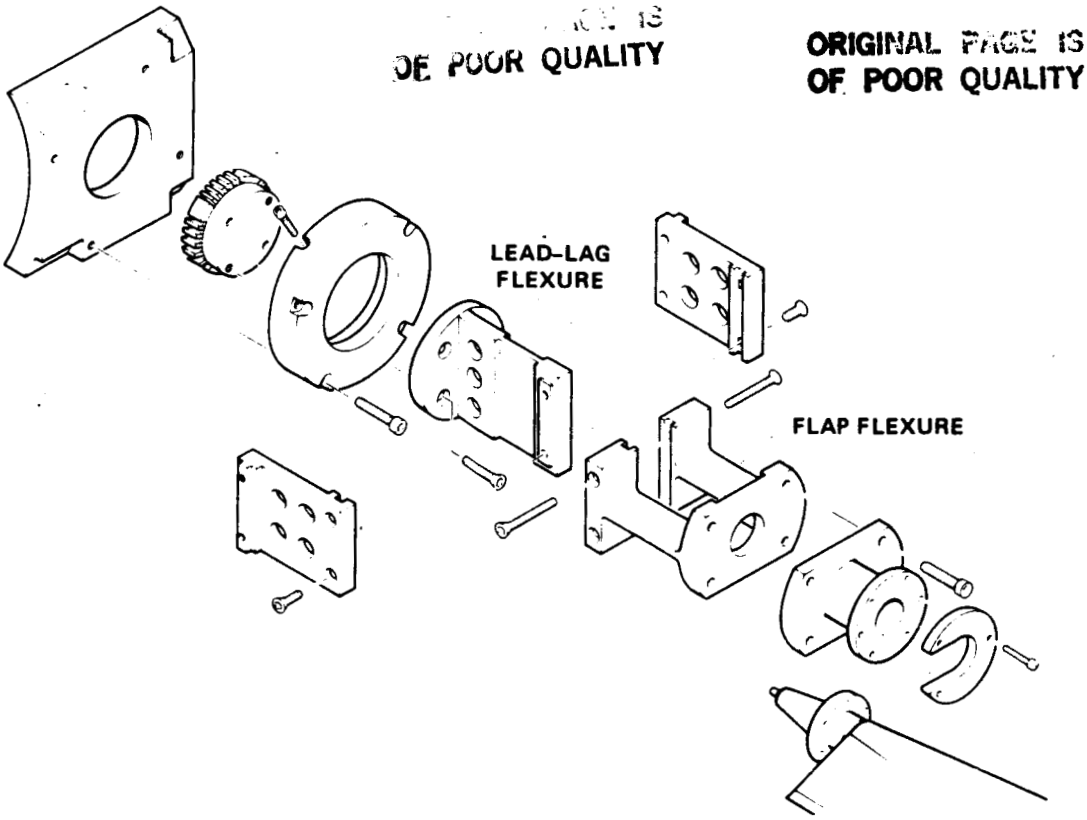

Figure 1. Exploded view of model flexure.

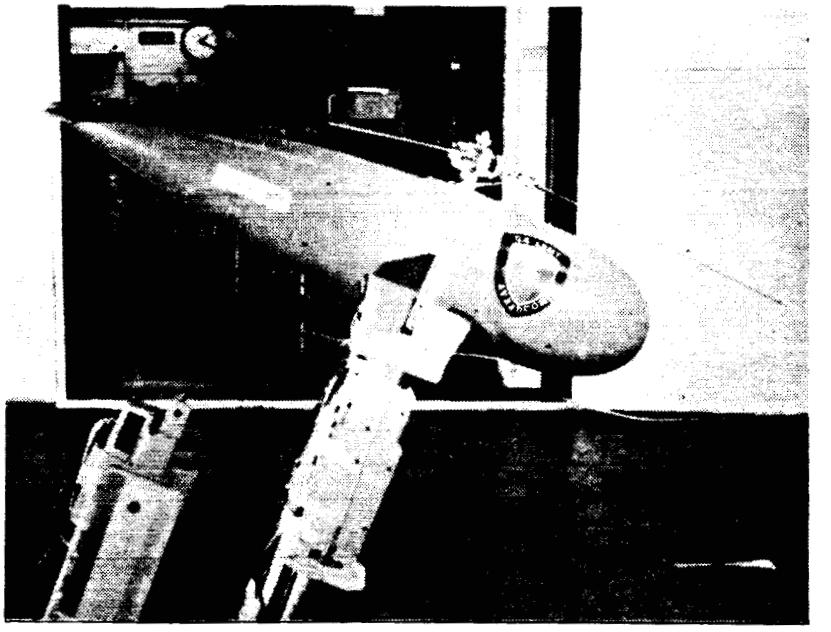

Figure 2. Model installed in the aeromechanics laboratory's 7-by-10-foot wind tunnel.

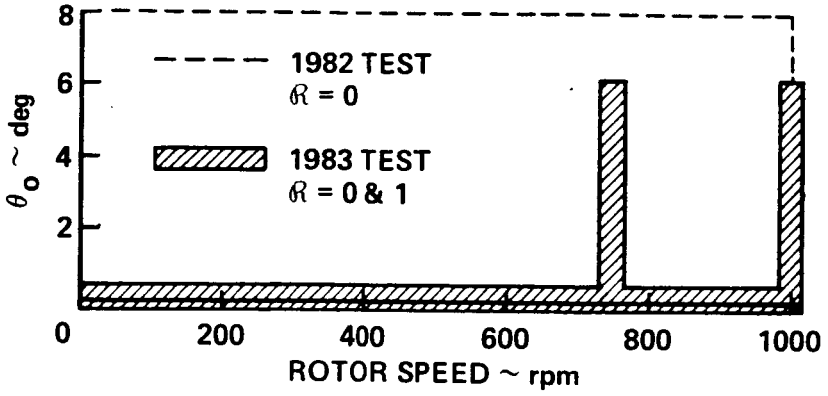

3(a) Hover tests.

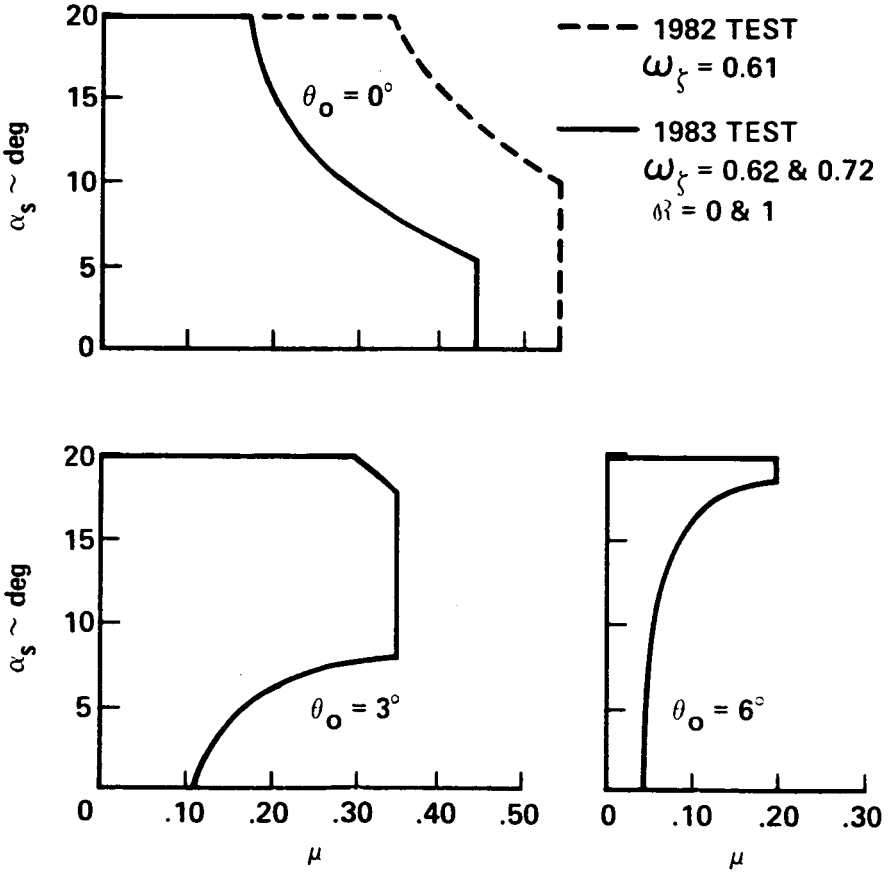

3(b) Forward flight tests.

Figure 3. Conditions tested.

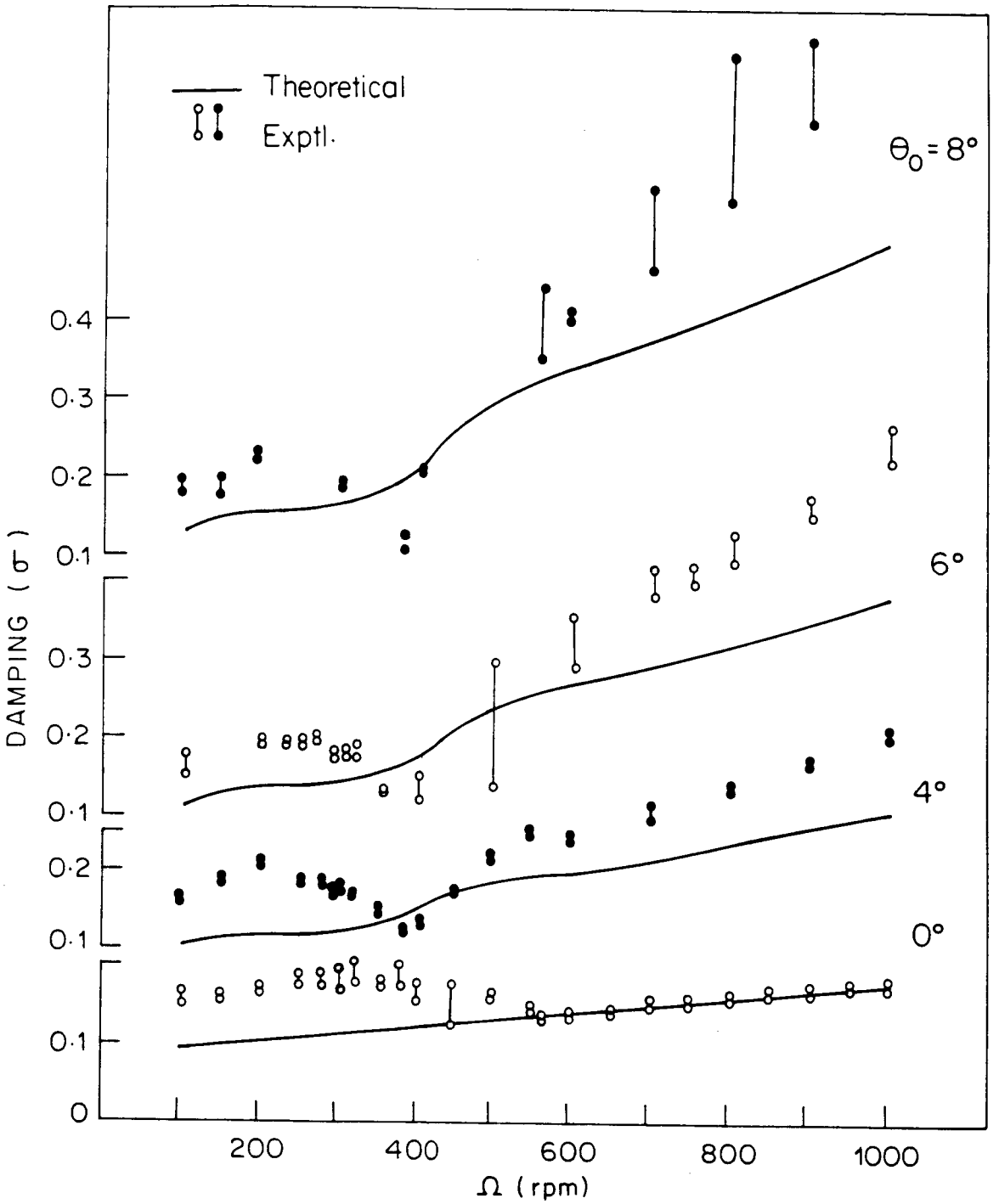

FIG. 4 LAG REGRESSING MODE DAMPING IN HOVER

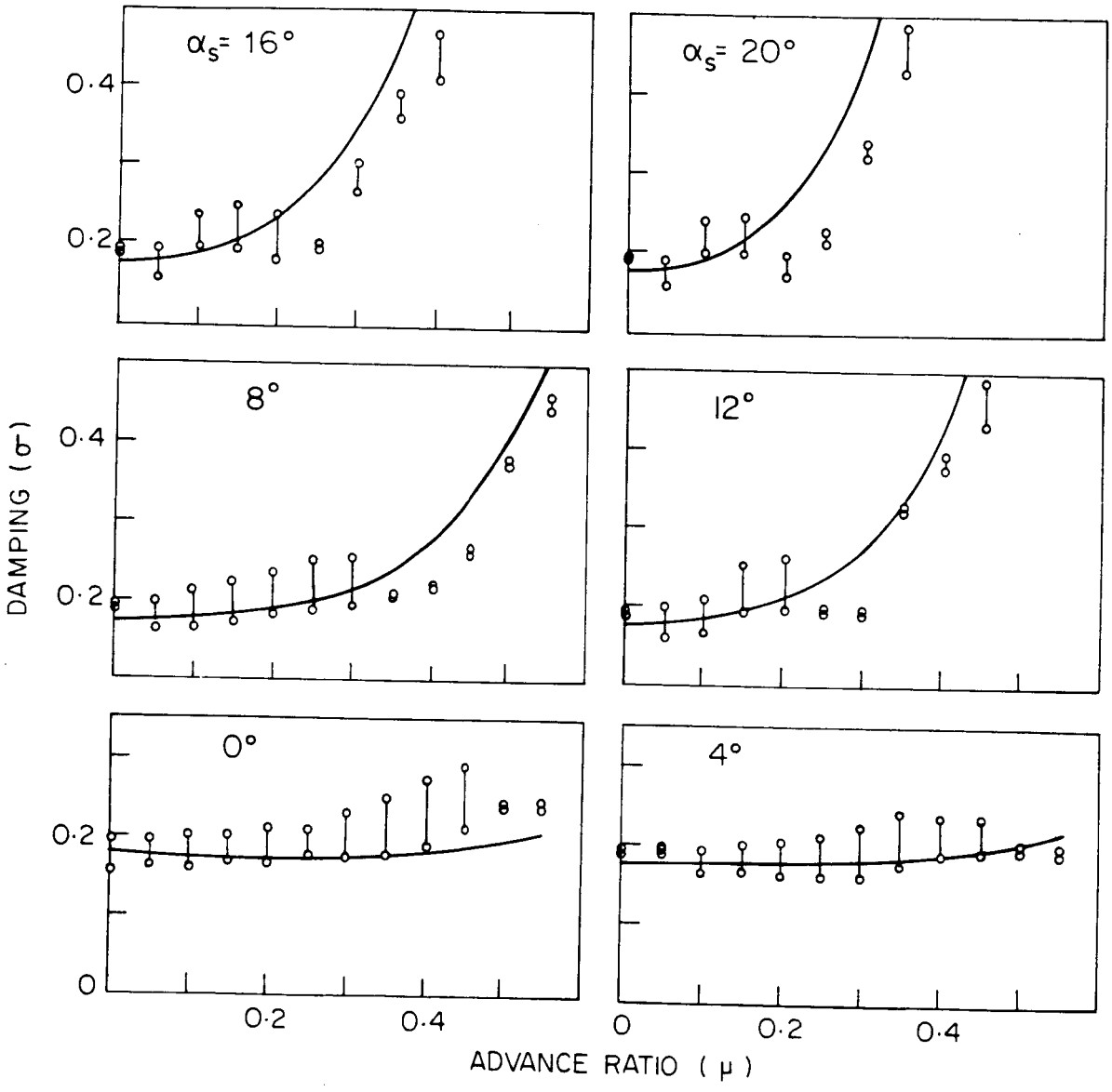

FIG. 5. LAG REGRESSING MODE DAMPING, θ_0= 0°, Ω=1000, R = 0
(THEORETICAL——, EXPTL. ⚲)

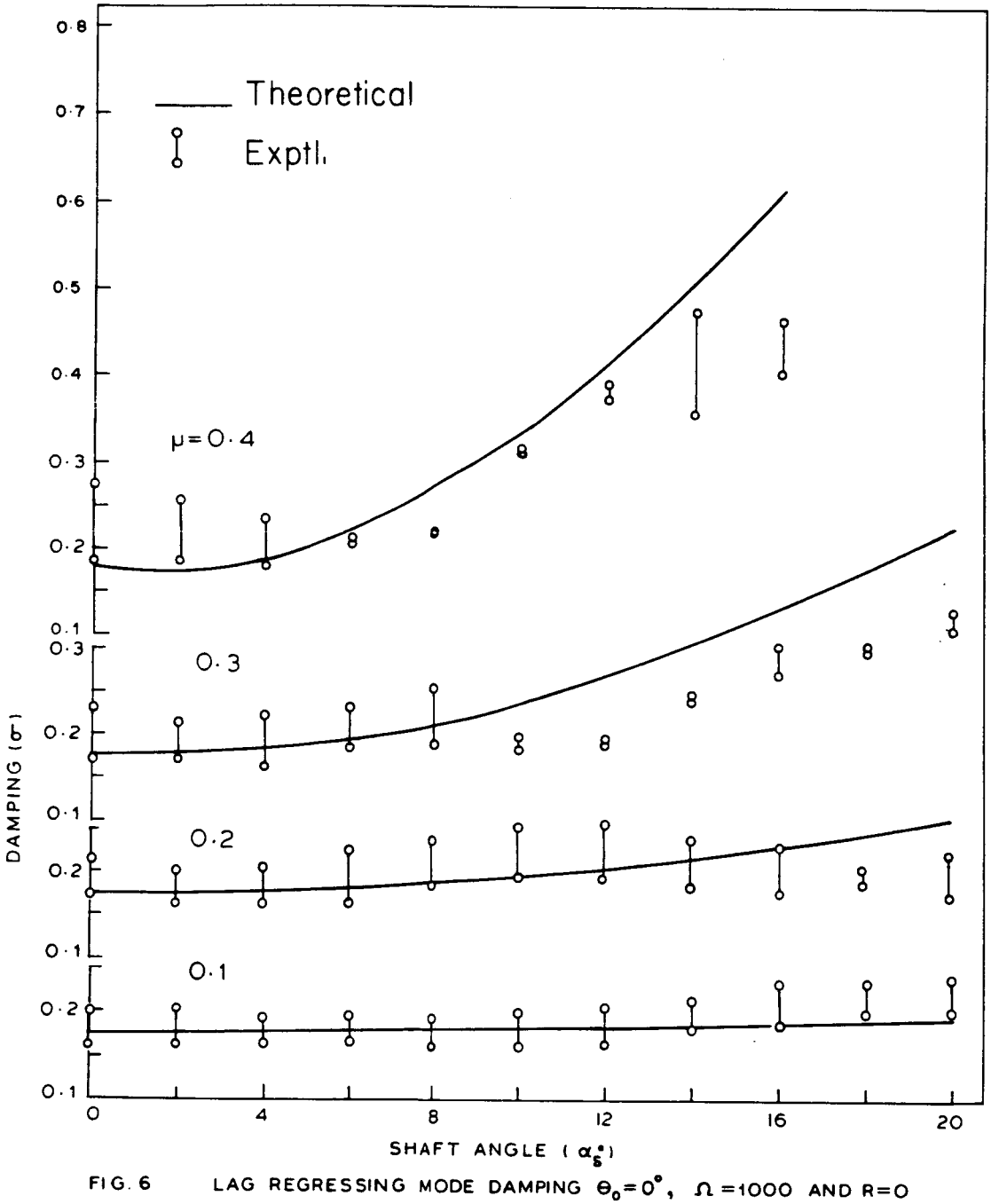

FIG. 6 LAG REGRESSING MODE DAMPING $\theta_0 = 0^\circ$, $\Omega = 1000$ AND R=0

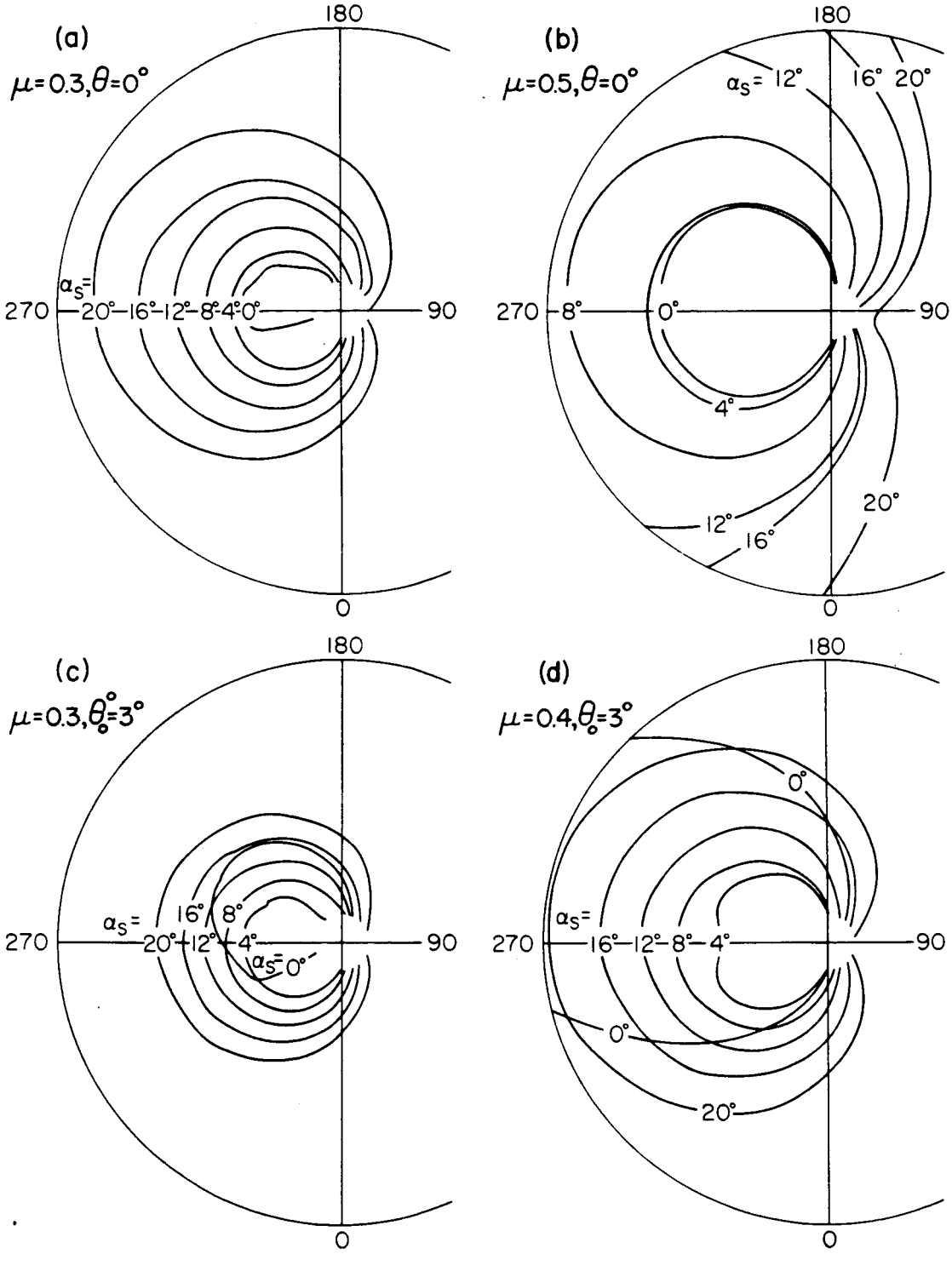

Fig. 7 STALL REGIONS, Ω=1000 RPM

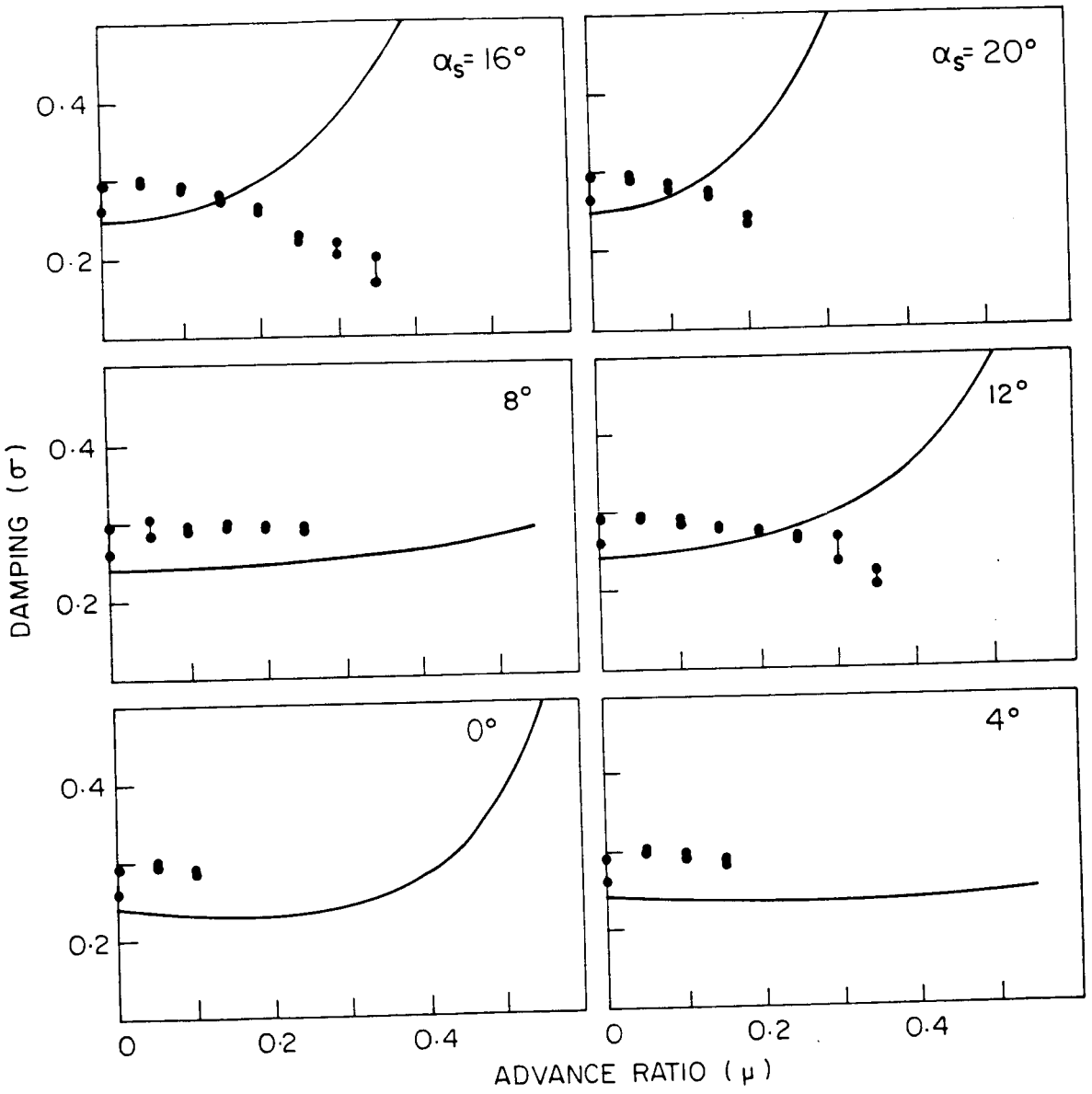

FIG. 8 LAG REGRESSING MODE DAMPING $\theta_0 = 3°$, R = 0, Ω = 1000
(THEORETICAL——, EXPTL. ⚲)

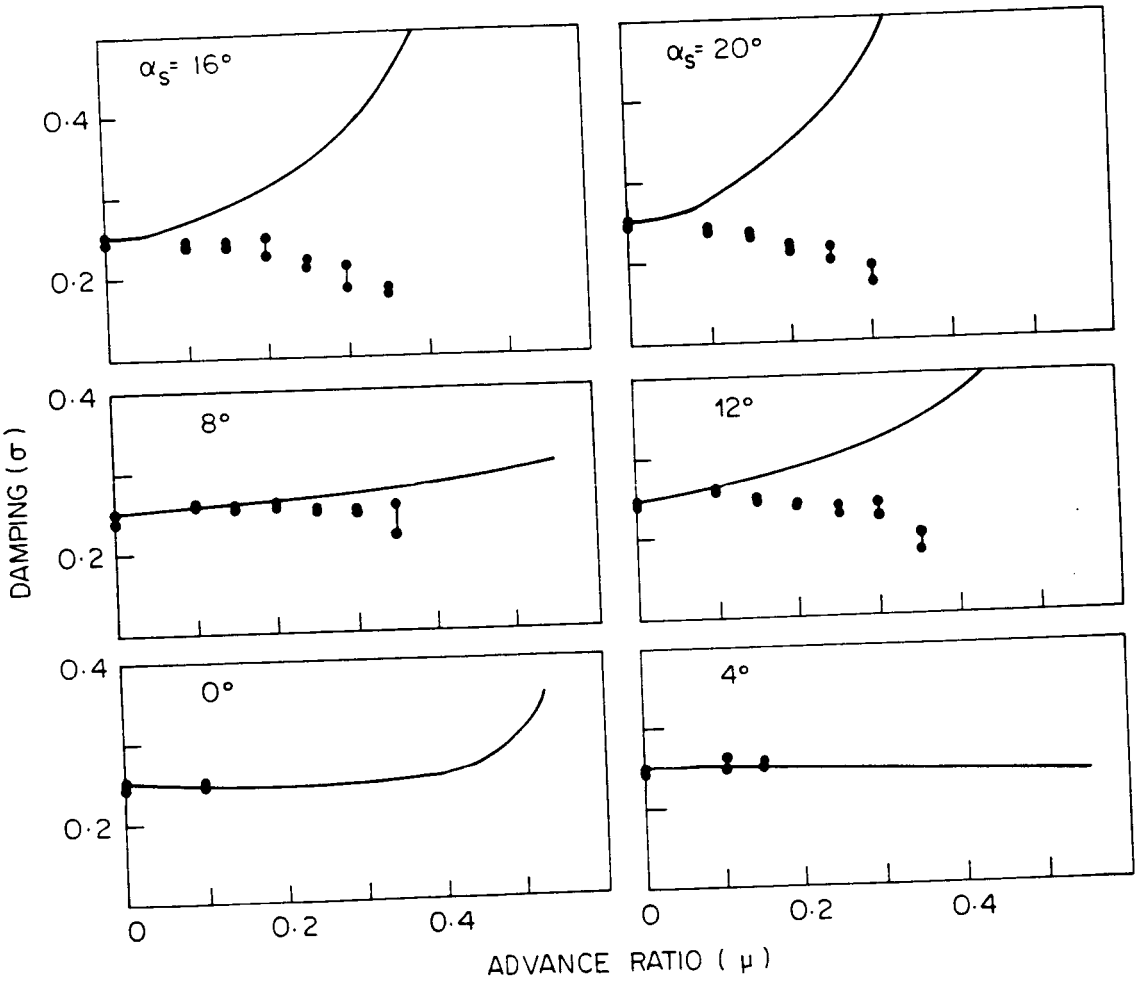

FIG. 9 LAG REGRESSING MODE DAMPING $\theta_0 = 3°$, $\Omega = 750$, $R = 1$
(THEORETICAL ——— , EXPERIMENTAL ⟟)

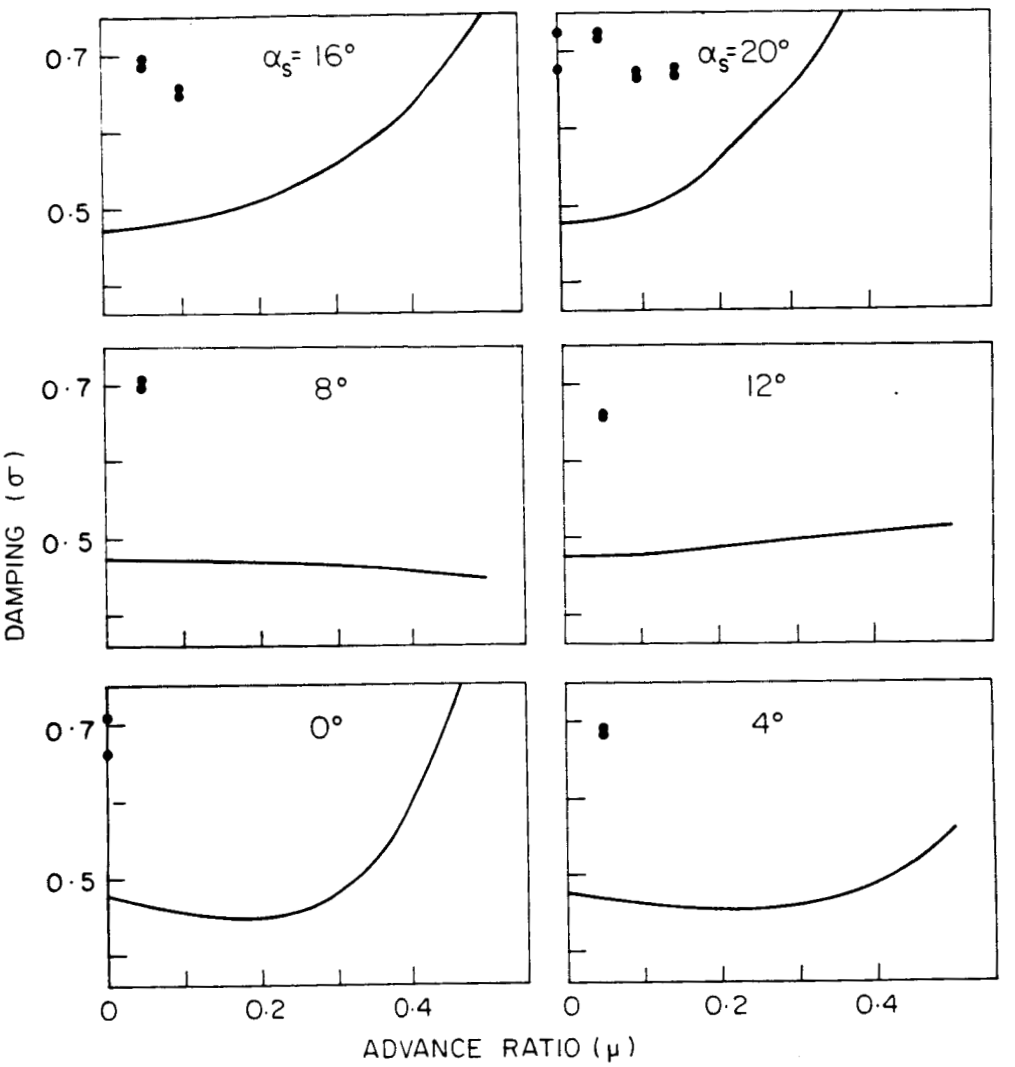

FIG. 10 LAG REGRESSING MODE DAMPING $\theta_0 = 6°$, $\Omega = 1000$, $R = 1$
(THEORETICAL ——, EXPERIMENTAL ⟟)

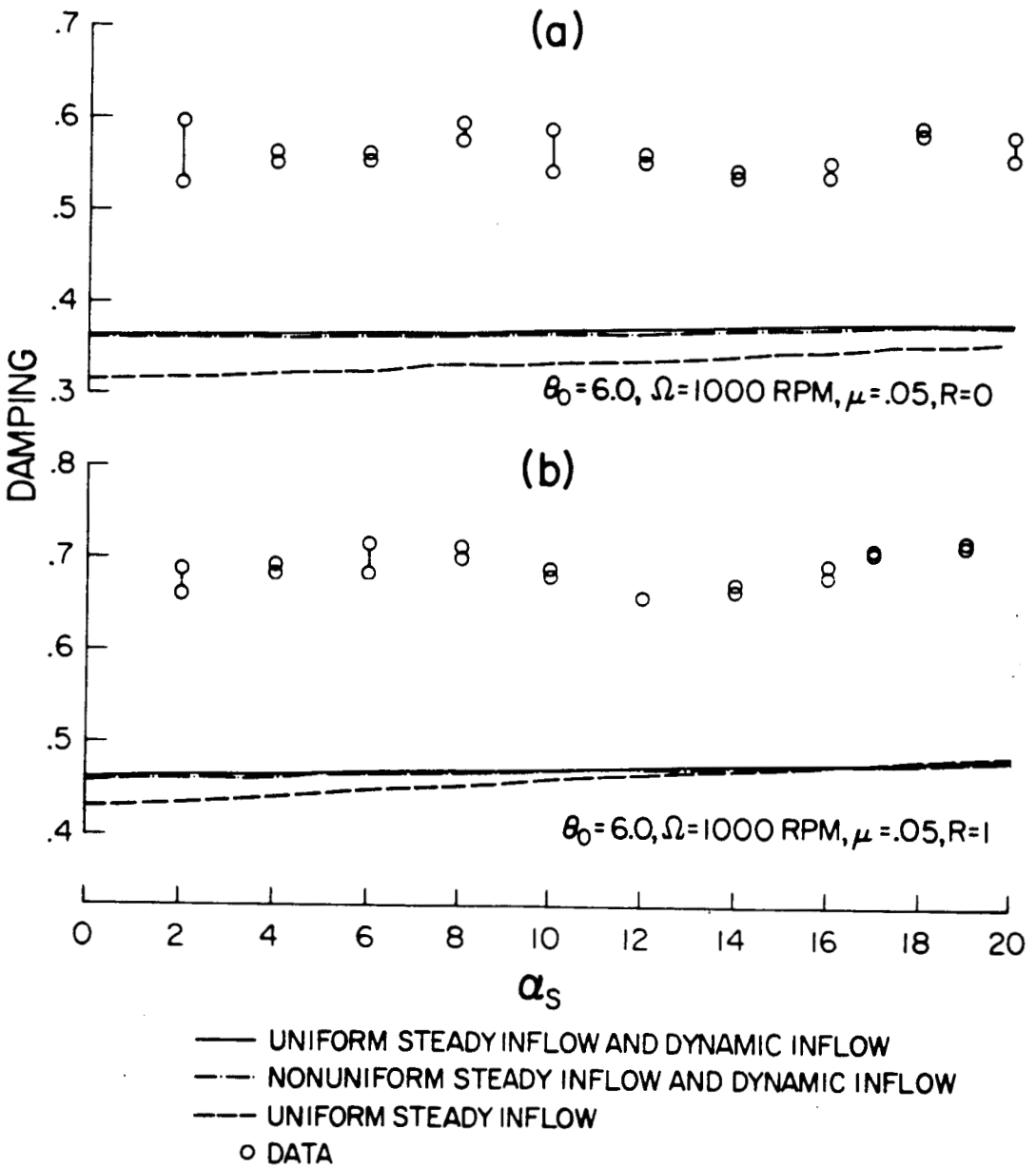

Fig. 11 LAG REGRESSING MODE DAMPING

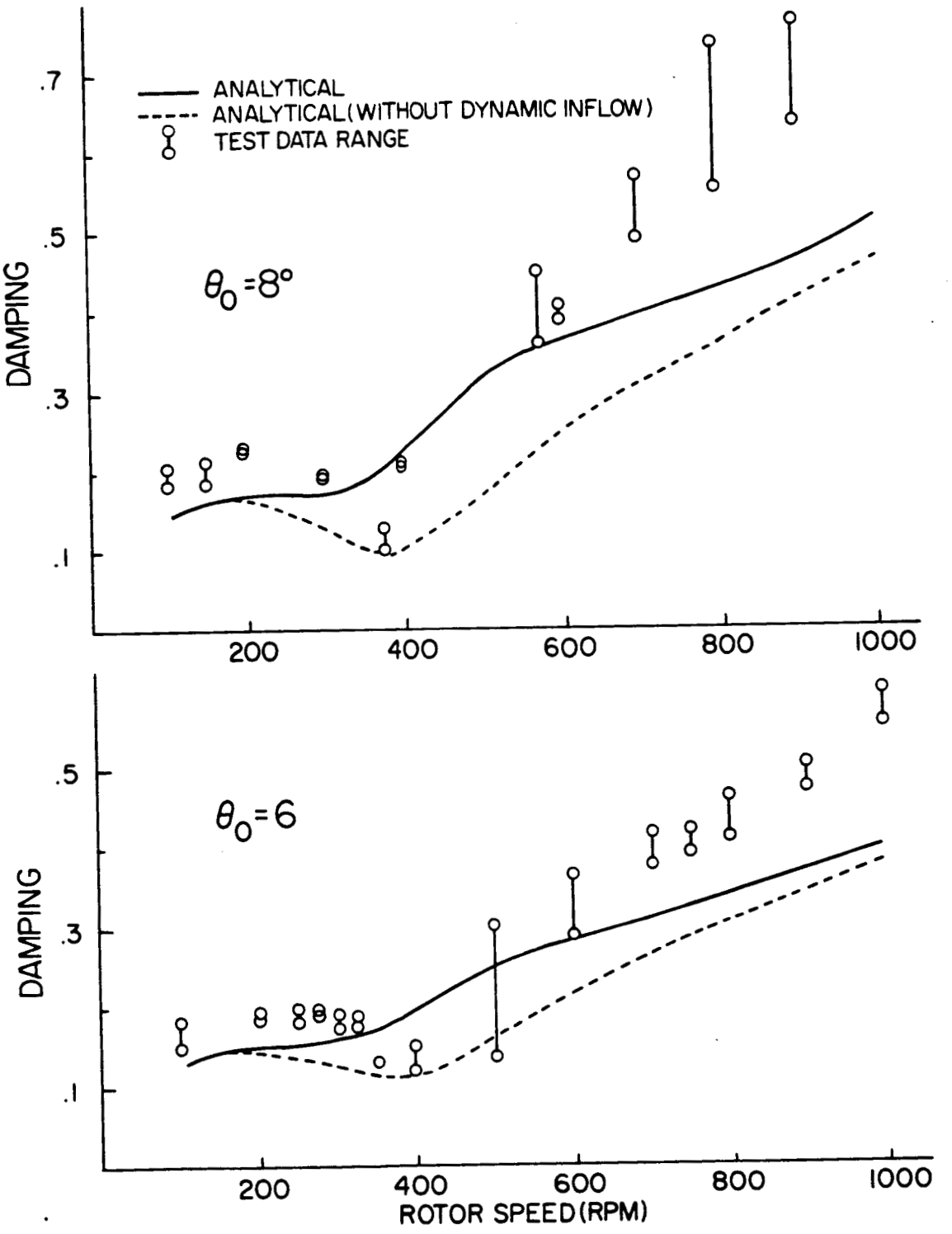

Fig. 12 CORRELATION OF MEASURED LAG REGRESSING MODE DAMPING WITH PREDICTED VALUES IN HOVER

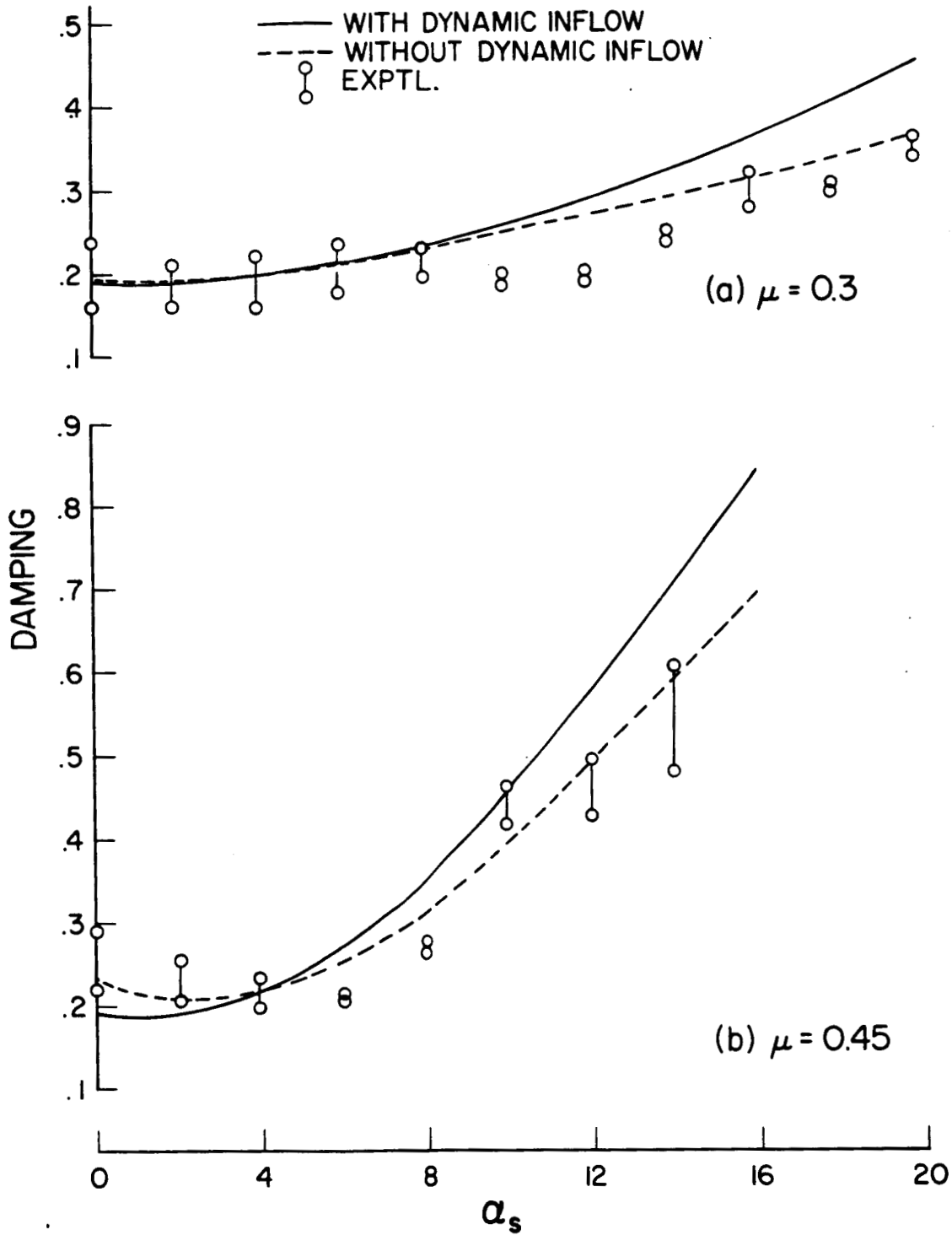

Fig. 13 LAG REGRESSING MODE DAMPING CORRELATIONS, IN SUBSTALL AND STALL (Ω=1000 RPM, R=0, θ_o= 0°)

Part 2 - Stall Effects

ABSTRACT

Experiments have been performed with a 1.62m diameter hingeless rotor in a wind tunnel to investigate flap-lag stability of isolated rotors in forward flight. The three-bladed rotor model closely approaches the simple theoretical concept of a hingeless rotor as a set of rigid, articulated flap-lag blades with offset and spring restrained flap and lag hinges. Lag regressing mode stability data was obtained for advance ratios as high as 0.55 for various combinations of collective pitch and shaft angle. The prediction includes quasi-steady stall effects on rotor trim and Floquet stability analyses. Correlation between data and prediction is presented and is compared with that of an earlier study based on a linear theory without stall effects. While the results with stall effects show marked differences from the linear theory results, the stall theory still falls short of adequate agreement with the experimental data.

NOMENCLATURE

a	Linear lift curve slope
c	Blade chord
$c_l(\alpha)$	Lift coefficient at α
$c_d(\alpha)$	Drag coefficient at α
c_{lo}	Lift coefficient at $\bar{\alpha}$
c_{do}	Drag coefficient at $\bar{\alpha}$
$c_{l\alpha o}$	Slope of the lift-coefficient curve at $\bar{\alpha}$

$c_{d\alpha o}$	Slope of the drag-coefficient curve at $\bar{\alpha}$
d	Drag force per unit length of the blade
e	Hinge offset/R
F_{yk}	Force per unit length of the k-th blade in the plane of rotation
F_{zk}	Force per unit length of the k-th blade in the plane perpendicular to the plane of rotation
I	Blade moment of inertia
l	Lift force per unit length of blade
$p_1, p_2, \cdot\cdot, p_{10}$	Coefficients as defined in equation (13)
R	Rotor blade radius or flap-lag structural coupling parameter
r	Spanwise station from hinge
U	Resultant flow velocity at a blade section/(ΩR)
U_P	Transverse velocity component/(ΩR)
U_T	Tangential velocity component/(ΩR)
U_{Po}	Trim-state transverse velocity component/(ΩR)
U_{To}	Trim-state tangential velocity component/(ΩR)
α	Blade section angle of attack
$\bar{\alpha}$	Trim-state blade section angle of attack
α_s	Shaft-tilt or shaft angle
β	Flapping angle of the blade
γ	Lock number, $\rho a c R^4/I$
ζ	Lead-lag angle of the blade
ΔU_P	Perturbed transverse velocity component/(ΩR)
ΔU_T	Perturbed tangential velocity component/(ΩR)
$\Delta\alpha$	Incremental angle of attack, $\alpha-\bar{\alpha}$.
θ_o	Collective blade pitch
ϕ	Local inflow angle
$\bar{\phi}$	$\mathrm{Tan}^{-1}(U_{Po}/U_{To})$
ϕ_o	U_{Po}/U_{To}
ρ	Air density
Ω	Rotor speed
ω_ζ	Dimensionless rotating lag frequency/Ω
λ	Total inflow ratio, $\lambda_i + \mu \tan\alpha_s$
λ_i	Induced flow due to thrust
μ	Advanced ratio
ψ_k	Azimuth angle of the k-th blade

$(\dot{})$ $\frac{d}{d\psi}(\ )$

INTRODUCTION

In an earlier study[1] we presented a correlation between data and prediction for flap-lag stability in forward flight. The correlation was based on a comprehensive data base on the lag regressing mode damping of an isolated rotor with three blades. Virtually rigid flap-lag blades were used, and the data base included aerodynamically demanding test cases with advance ratio, μ, as high as 0.55 and shaft-tilt angle, α_s, as high as 20°. The prediction was based on a linear quasi-steady aerodynamics theory with dynamic inflow. Overall, the prediction was found to be adequate for very low values of collective pitch, but deteriorated at the higher pitch angles. References 2 and 3, though restricted to hovering conditions, showed that inclusion of quasi-steady, nonlinear airfoil characteristics (stall effects) significantly improves correlation. The purpose of this continuing study is to investigate the effects of nonlinear airfoil characteristics under more demanding forward flight conditions.

In forward flight the number of correlation studies based on models that are intentionally simplified to isolate one aspect of the overall rotor stability problem are limited. Specifically stated, the structural simplicity of a rigid blade model facilitates isolation of aerodynamic effects. For an improved picture of airfoil effects, we now investigate the effects of nonlinear local lift, of nonlinear local drag and of profile drag at zero angle of attack. Furthermore, the correlation includes different combinations of pitch settings ($o \leq \theta_o \leq 8°$), advance ratios ($o \leq \mu \leq o{\cdot}55$) and shaft-tilt angles ($o \leq \alpha_s \leq 20°$) and thus provides a range of rotor loading conditions in forward flight.

EXPERIMENT AND DATA

For completeness, we include a brief account of the experimental model, for details see reference 1. To ensure the validity of using a simple flap-lag analysis for correlations, the three-bladed rotor used flexures to simulate articulated blades with spring restraint and coincident flap and lag hinges. The effective hinge offset was 0.11R. The blades were stiff relative to the flap and lag flexures so that the first flap and lag modes essentially involve only rigid body blade motions. Further, the design insures a rotating first

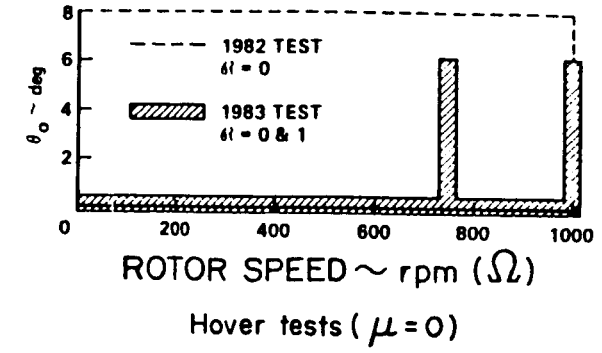

Hover tests ($\mu = 0$)

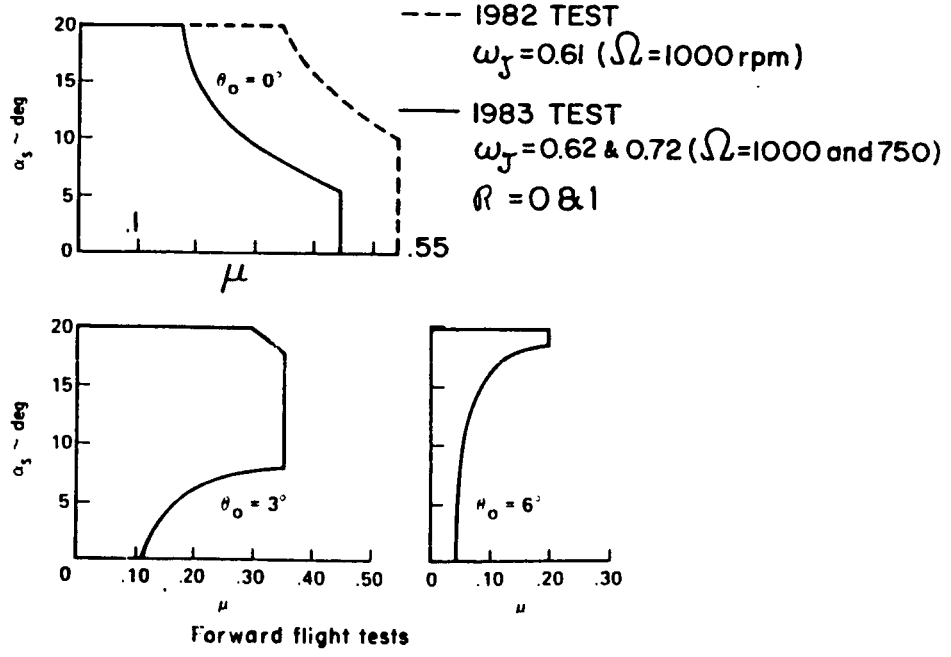

Forward flight tests

Figure 1b: Conditions tested

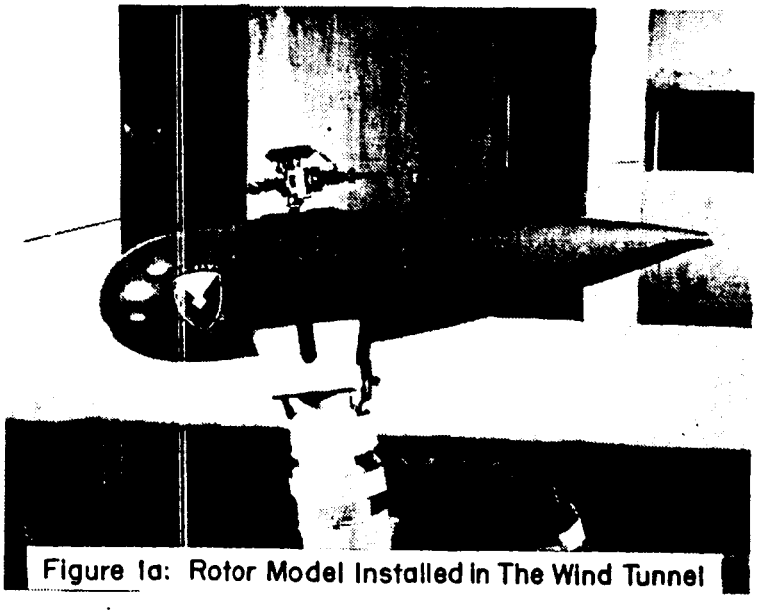

Figure 1a: Rotor Model Installed in The Wind Tunnel

Figure 1: Rotor Model Installed in The Wind Tunnel, and Hovering and Forward Flight Conditions Tested.

torsional frequency of at least 9/Rev over the entire rotor speed range tested, and thus virtually eliminating the need to consider a torsional degree of freedom. The measured and assumed parameter values of the test model are given in table 1.

The model tested was a 1.62m diameter three-bladed hingeless rotor mounted on a very stiff rotor stand so that the stability data was representative of an isolated rotor, see Fig. 1a. The rotor had no cyclic-pitch control and collective pitch was set manually prior to each run. At a given advance ratio, rotor speed and collective pitch the shaft tilt was the only means of controlling the rotor. Thus the rotor was operated untrimmed with an unrestricted tilt of the tip-path plane. The model was shaken in roll to excite the lag modes, and was then locked up and the transient response recorded. The frequency and damping data were then obtained from the time histories via the moving block technique. In forward flight two rotor speeds were used (Ω = 750 and 1000 rpm) corresponding to ω_ζ values of 0.62 and 0.72. Advance ratio, shaft-tilt angle and collective pitch were varied to cover the test envelope shown in figure 1b. At each condition tested at least two separate damping measurements were obtained.

Table 1: Model Properties

Number of blades	3
Radius	0.81 m
Chord	0.0419 m
Airfoil section	NACA 23012
Lift curve slope a	5.73
Profile drag coefficient at zero angle of attack (assumed)	0.0079 and 0.012
Nondimensional hinge offset	0.111
Blade inertia about hinge	0.01695 kg-m^2
Blade mass center distance from hinge	0.188m
Blade mass (Outboard of hinge)	0.204 kg
Nonrotating flap frequency	3.09 Hz
Nonrotating lead-lag frequency	7.02 Hz
Average lead-lag structural damping ratio	0.185% critical
Lock number γ (based on a=5.73)	7.54

ANALYSIS

The analytical model consists of an articulated rigid-blade flap-lag model with flap and lag spring restraints at the offset hinge. The hinge offset of 11.1% in flap and lag is accounted for in both the rotor trim and stability analyses. The rotor used no cyclic pitch so that at a given advance ratio, the collective pitch and the shaft tilt angles are the known trim parameters. The analytical model has the capability to include stall effects in both the rotor trim (zero cyclic pitch, and cyclic flapping present) and Floquet stability analyses. At an azimuth angle ψ_k, we consider a blade element of length dr of the k-th blade. The corresponding resultant flow velocity U and inflow angle ϕ in terms of normal and tangential velocity components are given by

$$U = \sqrt{U_T^2 + U_P^2} \approx U_T(1+\tfrac{1}{2}U_P^2/U_T^2) \tag{1}$$

$$\phi = \tan^{-1} U_P/U_T \tag{2}$$

The force components parallel and perpendicular to the plane of rotation are as follows:

$$dF_{yk} = (-l \sin\phi - d\cos\phi)dr \tag{3(a)}$$

$$dF_{zk} = (l\cos\phi - d\sin\phi)dr \tag{3(b)}$$

where

$$l = \tfrac{1}{2}\rho c\Omega^2 R^2 U^2 c_l(\alpha) \tag{4(a)}$$

$$d = \tfrac{1}{2}\rho c\Omega^2 R^2 U^2 c_d(\alpha) \tag{4(b)}$$

For a pitch setting θ_0 and trim angle of attack $\bar{\alpha}$, we have

$$\alpha = \theta_0 - \phi \text{ and } \bar{\alpha} = \theta_0 - \bar{\phi} \tag{6}$$

where

$$\bar{\phi} = \tan^{-1} U_{P0}/U_{T0} \tag{7}$$

The perturbation angle of attack $\Delta\alpha$ about $\bar{\alpha}$ is expressed as

$$\alpha - \bar{\alpha} = \Delta\alpha = \bar{\phi} - \phi \tag{8}$$

$$\approx \phi_0 - \frac{\phi_0^3}{3} - \frac{U_P}{U_T} + \frac{U_P^3}{3U_T^3}$$

Expanding $c_l(\alpha)$ and $c_d(\alpha)$ about $\bar{\alpha}$ we get

$$c_l(\alpha) = c_l(\bar{\alpha}) + \left(\frac{dc_l}{d\alpha}\right)_{\bar{\alpha}} (\alpha - \bar{\alpha}) \tag{9a}$$

$$c_d(\alpha) = c_d(\bar{\alpha}) + \left(\frac{dc_d}{d\alpha}\right)_{\bar{\alpha}} (\alpha - \bar{\alpha}) \tag{9b}$$

Similarly substituting equations 1, 4 and 9 in equation 3, we get

$$dF_{yk} = \tfrac{1}{2}\rho c R^2 \Omega^2 U\{ - (c_{do} + c_{d\alpha o}\Delta\alpha)\, U_T - (c_{lo} + c_{l\alpha o}\Delta\alpha) U_P\} dr \tag{10a}$$

$$dF_{zk} = \tfrac{1}{2}\rho c R^2 \Omega^2 U\{ - (c_{do} + c_{d\alpha o}\Delta\alpha)\, U_P + (c_{lo} + c_{l\alpha o}\Delta\alpha) U_T\} dr \tag{10b}$$

where

$$U_P = e \cos\zeta + \cos\beta\,(1 + \dot{\zeta}) r/R + \mu \sin(\psi + \zeta) \tag{11}$$

$$U_T = e \sin\zeta \sin\beta + r\dot{\beta}/R + \lambda \cos\beta + \mu \sin\beta \cos(\psi + \zeta)$$

Now we perturb the total velocity component about the trim state. That is

$$U_P = U_{Po} + \Delta U_T \tag{12}$$

$$U_T = U_{To} + \Delta U_T$$

Substituting equations 1, 8 and 12 in equation 10 and neglecting the products of perturbation quantities such as ΔU_T^2, we get

$$dF_{yk} = \tfrac{1}{2}\rho c \Omega^2 R^2 U\{ p_1 U_T^2 + p_2 U_T U_P + p_3 U_P^2 + p_4 U_P \Delta U_P + p_5 U_P \Delta U_T\} dr, \tag{12a}$$

$$dF_{zk} = \tfrac{1}{2}\rho c \Omega^2 R^2 U\{p_6 U_T^2 + p_7 U_T U_P + p_8 U_P^2 + p_9 U_P \Delta U_P + p_{10} U_P \Delta U_T\} dr, \tag{12b}$$

where

$$p_1 = \{ - c_{do} - c_{d\alpha o}(\phi_o - \frac{\phi_o^3}{3}) \} \tag{13}$$

$$p_2 = \{ c_{d\alpha o} - c_{lo} - c_{l\alpha o}(\phi_o - \frac{\phi_o^3}{3}) \}$$

$$p_3 = \{ - 1/2\, c_{do} - \frac{c_{d\alpha o}\phi_o}{3} - 1/2\, \phi_o c_{lo} + c_{l\alpha o}(1 - \frac{\phi_o^3}{3}) \}$$

$$p_4 = \{ c_{d\alpha o}\,(1/6\, \phi_o - 1/2\, \phi_o^3) - 1/2\, \phi_o c_{lo} - c_{l\alpha o} \frac{\phi_o^2}{6} \}$$

$$p_5 = \{ -\frac{c_{d\alpha o}\,\phi_o^2}{6} + c_{lo}\,\frac{\phi_o^2}{2} + \frac{1}{6}\,c_{l\alpha o}\phi_o^3 \}$$

$$p_6 = \{ c_{lo} + c_{l\alpha o}(\phi_o - \frac{1}{3}\,\phi_o^3) \}$$

$$p_7 = \{ -c_{l\alpha o} - c_{do} - c_{d\alpha o}\,(\phi_o - \frac{1}{3}\phi_o^3) \}$$

$$p_8 = \{ \frac{c_{lo}}{2} + \frac{c_{l\alpha o}\phi_o}{3} - \frac{c_{do}\phi_o}{2} + c_{d\alpha o}\,(1 - \frac{1}{3}\,\phi_o^3\,) \}$$

$$p_9 = \{ -c_{l\alpha o}(1/6 - \frac{\phi_o^3}{3}) - \frac{c_{do}\phi_o}{2} - \frac{c_{d\alpha o}\phi_o^2}{6} \}$$

$$p_{10} = \{ \frac{c_{l\alpha o}\phi_o^2}{6} - \frac{c_{do}\phi_o^2}{2} + \frac{c_{d\alpha o}\phi_o^3}{6} \}$$

We observe that the quantities $c_{l\alpha o}$, $c_{d\alpha o}$, c_{lo} and c_{do} in p_1, p_2,..,p_{10} experience large variations in numerical values and that the derivation is carried out in terms of p_1,..,p_{10} throughout (that is without breaking the p quantities in terms of individual components). Further we stipulate that p_1....p_{10} are of order unity in deriving the equations. The subsequent derivation of the flap-lag-dynamic inflow equation follows reference 1 except for the following difference. At any azimuth station, we integrate the aerodynamic terms numerically along blade span since c_{lo}, $c_{l\alpha o}$, c_{do}, $c_{d\alpha o}$ are complex functions of radial coordinate and azimuth.

To generate the equations, we use a special purpose symbolic processor DEHIM (Dynamic Equations of Helicopter Interpretive Models).[6,7] It also generates FORTRAN coded statements of the equations which are utilized to form subroutines. These subroutines are directly linked with numerical analysis program to facilitate evaluate the coefficients of the governing equations. The numerical analysis program evaluates the rotor trim parameters with stall characteristics, performs Floquet stability analysis and identifies the modes. The numerical integration of aerodynamic terms in the equations along the span is done by a 10 point Gaussian quadrature. We generate the Floquet transistion matrix by

subroutine DVERK(IMSL) which is a Runge-Kutta-Verner fifth and sixth order method. The program evaluates the four aerofoil characteristics c_{lo}, $c_{l\alpha o}$, c_{do} and $d_{d\alpha o}$ for any given angle of attack α by linear interpolation from a table with data at 5°intervals for $o \leq \alpha \leq 360°$. The airfoil characteristics used in this paper are shown in figure 2. For low angles of attack these are the same as the airfoil properties used in our earlier study[1] based on the linear theory except for the following difference. In reference 1, c_d (α = 0) = 0.0079 throughout. However, in the present study we consider two values of c_d (α = 0); 0.0079 as in references 2 and 3 and 0.012 as in references 4. With double precision arithmatic, the average CPU time for each case was about 5 minutes on VAX 750 computer.

Finally, we conclude this section with a note concerning the comparison between the numerical results from the stall theory and from the linear theory. For a consistent comparison for the entire test envelope, we compute the damping data from the stall theory and also from the same stall theory by suppressing the stall effects. The latter computations refer to the linear theory and compare with those in reference 1.

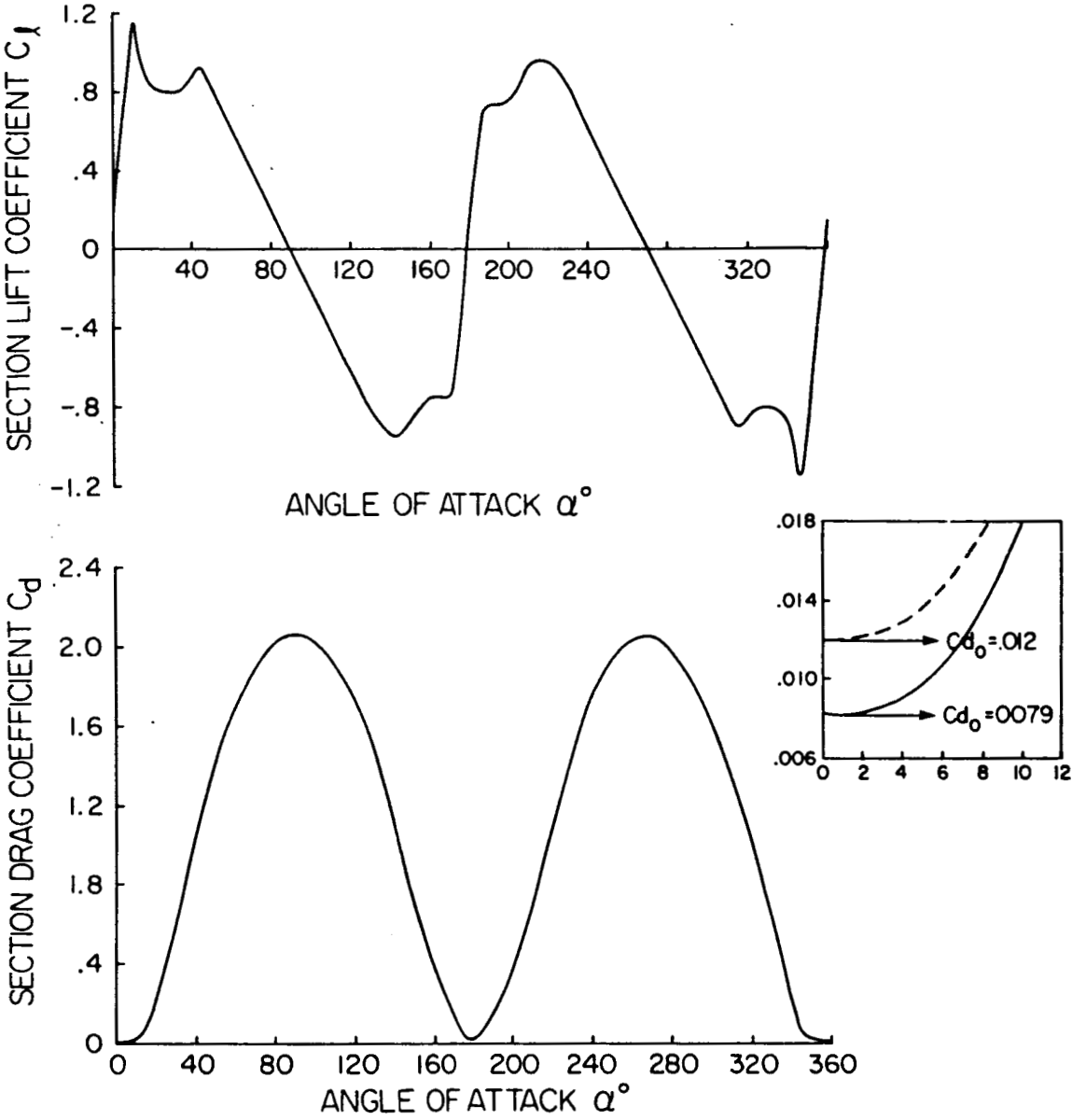

FIG. 2 ASSUMED NON-LINEAR LIFT AND DRAG CHARACTERISTICS OF AIRFOIL

RESULTS

We predict the lag regressing mode damping for the parameter values of the test model given in Table 1, covering the entire test envelope shown in figure 1b. We use two theories, the quasi-steady aerodynamics with dynamic inflow (linear theory) and the stall theory which is this linear theory refined to include nonlinear airfoil section local lift and drag characteristics in a quasi-steady manner. If not stated otherwise, the following convention and parameter values apply: full lines for predictions with linear theory, dotted lines for predictions with stall theory and c_d (α = o) = 0.0079, R = 0.0 and ω_ζ = 0.72 (Ω = 1000 rpm).

We begin the discussion of correlation with figure 3 which is for the hovering case for four values of the collective pitch setting θ_o° = 0, 4, 6 and 8. The improvement with inclusion of quasi-steady stall is marginal and it is due to nonlinear airfoil-section local drag coefficient (non-linear drag for short) in substall. This is expected because the angle of attack is low for all the four cases tested. For example at 0.7R, the approximate mean or trim angle of attack $\bar{\alpha}$ varies from 0° for θ_o° = 0, to 4° for θ_o° = 8. Overall the correlation is fair. However we observe two types of consistent underpredictions. For Ω < 300 rpm, the first type is observed for which the deviation from the data essentially remains the same with increasing pitch setting. For Ω > 700 rpm, the second type is observed for which the deviation increases with increasing θ_o. These deviations were found not to be associated with ground effect, recirculation and nonuniform steady inflow.[1] The present stall theory shows that the deviations are not associated with nonlinear drag. The deviations are surprising and merit further study. (The role of dynamic inflow with stall and of higher airfoil profile drag with c_d (α= 0) = 0.012 is discussed later).

We now present the forward flight case in figure 4 which shows the correlation for zero collective and for relatively low values of the shaft-tilt angle ($\alpha_s^\circ \leq 6$). For $\mu \leq 0.4$, both the theories show good agreement with the data for all the four cases, α_s° = 0, 2, 4, and 6. This is expected since the predictions refer to low thrust conditions due to zero pitch setting and low shaft-tilt angles. For $\mu > 0.4$ and α_s° = 4 and 6, the non-linear effects begin to affect the predictions.

To facilitate further discussion, we refer to the areas of the stall regions ($|\alpha| > 12°$) based on trim values as a means of quantifying stall effects. Stall plots are given in figure 5 including different combinations of θ_o and α_s

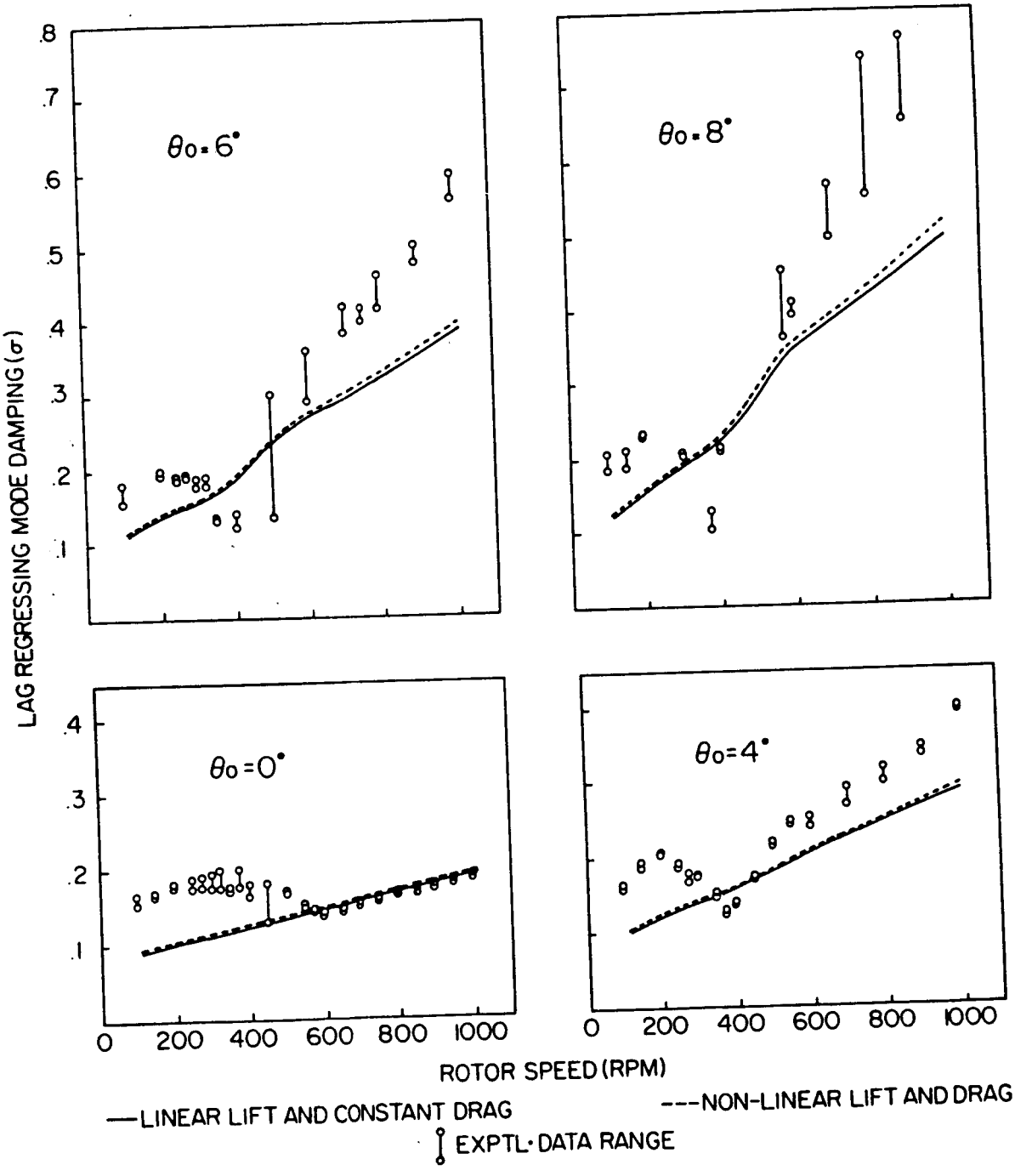

FIG.3 CORRELATION OF LAG REGRESSING MODE DAMPING WITH AND WITHOUT STALL EFFECTS IN HOVER

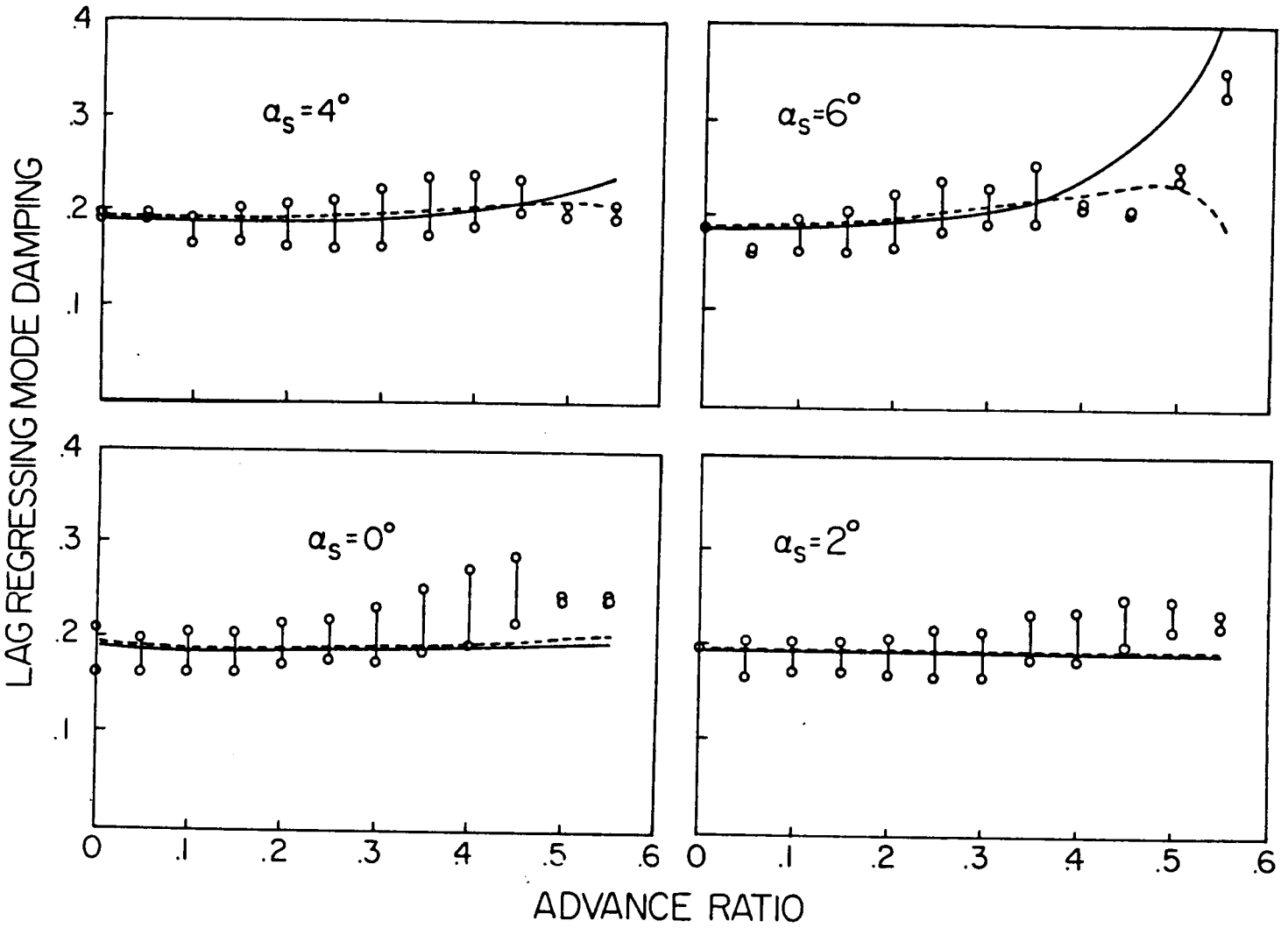

FIG. 4 CORRELATION OF LAG REGRESSING MODE DAMPING WITH AND WITHOUT STALL EFFECTS IN FORWARD FLIGHT FOR LOW SHAFT TILT ANGLES FOR $\theta_o = 0°$

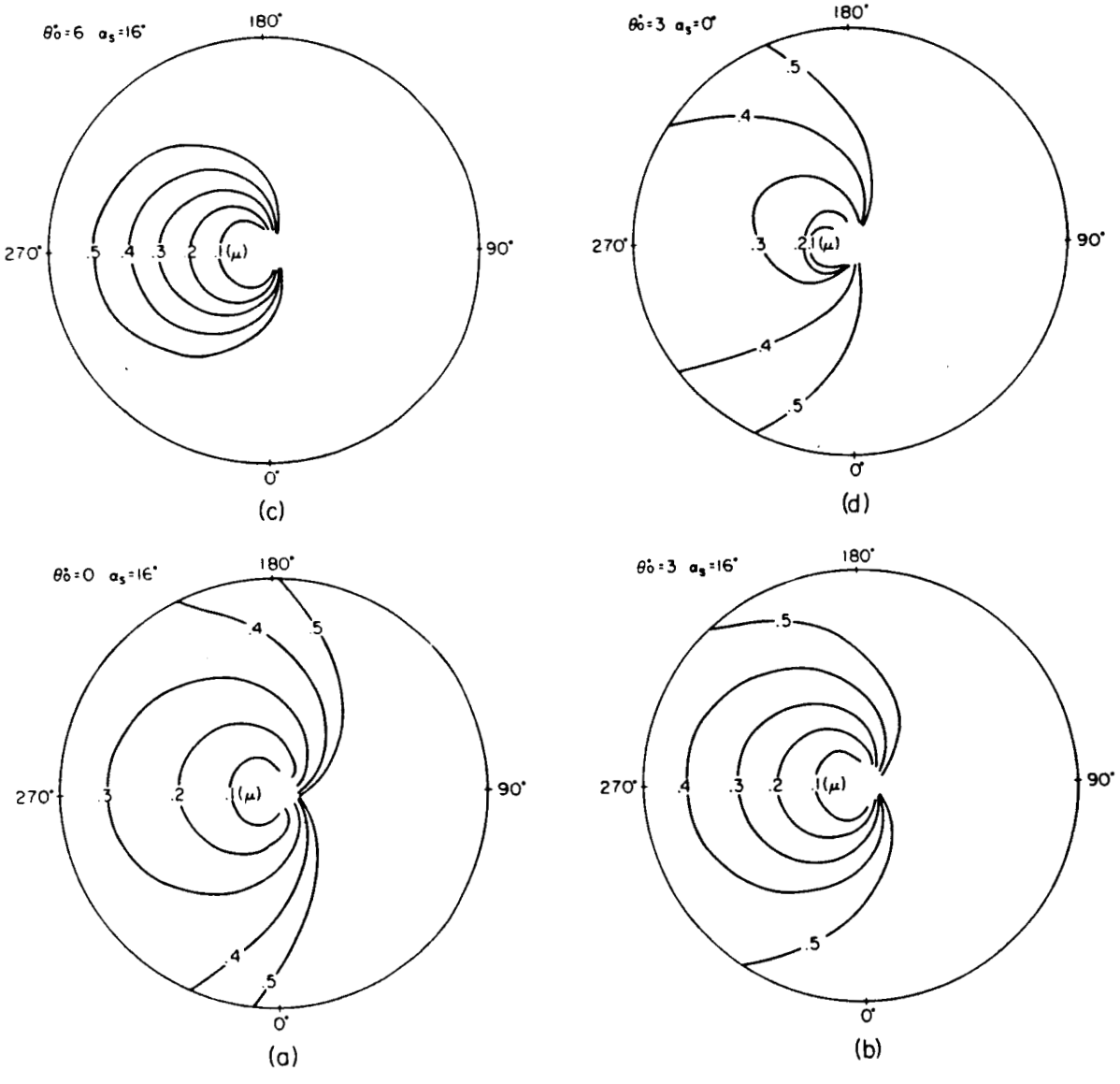

FIG.5 STALL REGIONS FOR VARIOUS ADVANCE RATIOS AND FOR $\theta_0^\circ = 0^\circ, 3^\circ$ AND 6°

for various μ values. We observe (not included in figure 5 but given reference 1) that 10% to 12% of the rotor disk is in stall for $\mu = .5$ and $\alpha_s° = 4$, and for $\mu = .4$ and $\alpha_s° = 6$, and that this percentage increases to 16-18 for $\mu = .5$ and $\alpha_s° = 6$. Overall, both the theories give good correlation. However, a qualitative aspect of the correlation merits special mention. The data point at $\mu = 0.55$ and $\alpha_s° = 6$ shows that the damping is increasing with increasing μ; a trend that is not captured by the stall theory. We should also mention that this trend is captured by the linear theory, although nearly 1/4 of the rotor disk is experiencing stall for $\mu = .55$ and $\alpha_s° = 6$.[1]

Figure 6 shows the correlation at the same zero collective pitch setting for higher values of the shaft-tilt angle ($8 \leq \alpha_s° \leq 20$) from hovering to high advance ratios ($o \leq \mu \leq .55$). Both the theories show close agreement with the data for all four cases ($\alpha_s° = 8$, 12, 16, and 20) when less than 10%-12% of the rotor disk is in stall.[1] Specifically, these ranges are: $\mu \leq .3$, $\alpha_s° = 8$; $\mu \leq .25$, $\alpha_s° = 12$; $\mu \leq .225$, $\alpha_s° = 16$, and $\mu \leq .175$, $\alpha_s° = 20$. They represent very low thrust conditions with negligible influence of nonlinear drag in substall. Moreover, the stall theory fails to capture the trend of the data (i.e., increasing damping with increasing μ) when more than 20-25% of the disk is in stall, as observed for the following ranges: $\mu > .425$, $\alpha_s° = 8$; $\mu > .325$, $\alpha_s° = 12$; $\mu > .3$, $\alpha_s° = 16$, and $\mu = 0.25$, $\alpha_s° = 20$. For the in-between cases when 12%-20% of the disk is in stall, the stall theory shows perhaps a slight improvement. Reiterating we summarize the correlations in figures 4 and 6 as follows. First, when more than about 20-25% of the disk is in stall, which occurs for high values μ and α_s, the stall theory does not capture the trend of the data. We suggest that dynamic stall may be contributing to this situation. It is not known why the linear theory gives better results here. Second, when less than about 10-12% of the disk is in stall, the stall theory is found to merge with the linear theory (low α values due to low values of pitch setting, μ and α_s). Third, between these two ranges the nonlinear theory seem to give slightly better results than the linear theory does, but this is not conclusively demonstrated by the nonlinear theory.

For the three-degree collective case, figure 7 shows the results for $0 \leq \mu \leq .55$ and $0 \leq \alpha_s° \leq 20$. The data shows the trend that the damping decreases smoothly with increasing values of μ and α_s ($\alpha_s \geq 12°$). The linear theory becomes qualitatively inaccurate with increasing μ and $\alpha_s°$ (≥ 12), showing the opposite trend of increasing damping with increasing μ. The stall theory, like the data shows an eventual damping reduction with increasing advance ratio, but the

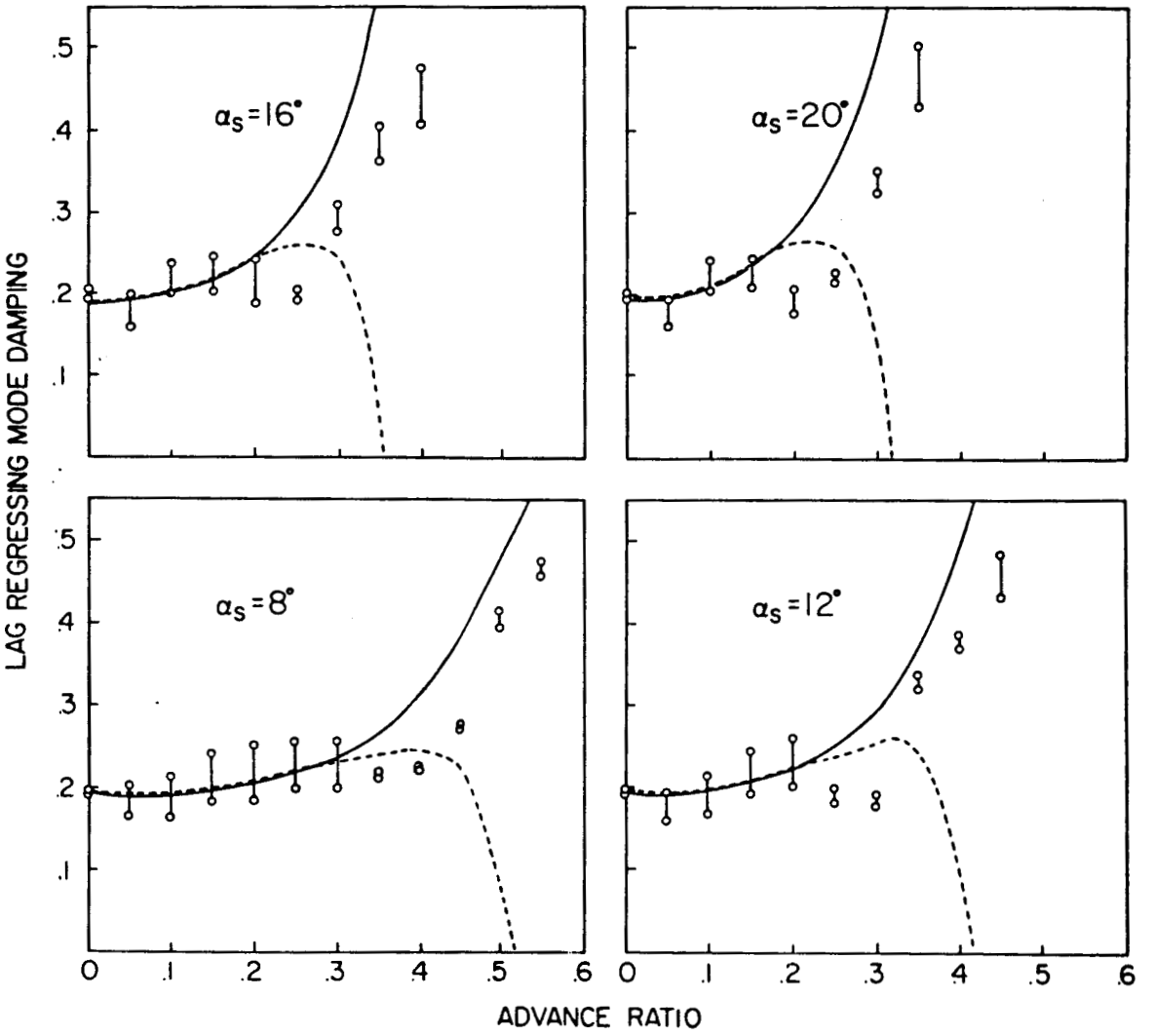

FIG.6 CORRELATION OF LAG REGRESSING MODE DAMPING WITH AND WITHOUT STALL EFFECTS IN FORWARD FLIGHT FOR HIGH SHAFT TILT ANGLES FOR θ_o=0°

FIG. 7 CORRELATION OF LAG REGRESSING MODE DAMPING WITH AND WITHOUT STALL EFFECTS IN FORWARD FLIGHT, θ_0 =3°

character of this reduction is quite different. For small values of shaft-tilt angle α_s° (≤ 8), the data is available for $\mu \leq .25$ and stall is hardly an issue. The minor differences between the two theories are due to nonlinear drag in substall. That the stall theory shows sudden decrease in damping at $\mu \approx .4$ for $\alpha_s^\circ = 0$ is likely due to sudden increase in stall effects, as seen from the stall plots in figure 5 for $\theta_0^\circ = 3$ and $\alpha_s^\circ = 0$. Further, as seen from figure 7 for $\alpha_s^\circ = 0$, 4, and 8, the difference between theory and data remains nearly the same as it was in hover. According to an earlier study, that difference was found not to be associated with nonuniform steady inflow (more discussion on this difference later in figure 13). For higher shaft-tilt angles ($\alpha_s^\circ \geq 12$) in figure 7 the stall effects are negligible for the following three ranges of data: $\mu \leq .275$, $\alpha_s^\circ = 12$; $\mu \leq .225$, $\alpha_s^\circ = 16$; and $\mu \leq .175$, and $\alpha_s^\circ = 20$. That is, less than 10-12% of the disk is in stall and there is negligible difference between the two theories. For the remaining three ranges of data with $\alpha_s^\circ \geq 12$, stall effects become increasingly important with increasing μ and α_s. For example, at $\mu = .35$ and $\alpha_s^\circ = 16$, nearly 25% of the disk is in stall. The stall theory substantially differs from the linear theory but still does not correlate well with the data.

Figure 8 shows the correlation for the six-degree collective case. Only a limited amount of data are available ($\mu \leq .15$) and stall is not an issue here (less than 10% of the disk experiences stall for the entire set of data, also see figure 5 for $\theta_0^\circ = 6$ and $\alpha_s^\circ = 16$). The behaviour of the theories relative to each other remains essentially as it was for the 3° collective case.

The predictions from the stall theory, as presented earlier, include the total stall effects of lift and drag. It is instructive to estimate how much of that total is due to nonlinear lift and how much, due to nonlinear drag. This question is addressed in figure 9 for hovering and in figure 10 for forward flight. The hovering case has eight degree collective treated earlier in figure 3, and substall conditions are present throughout ($\alpha \approx 4^\circ$ at .7R). We have shown predictions for four cases---linear lift and drag in combination with nonlinear local lift and drag -- as identified in the figure. Given the substall conditions, the nonlinear lift characteristics have no impact on the predictions. As expected, the predictions from the nonlinear lift-and-drag theory (stall theory) merges with those from the linear-lift and nonlinear-drag theory. The same is true of the other two predictions from the nonlinear-lift and constant-drag theory and the linear-lift and constant-drag theory (linear theory). Thus the relevant ingredient below stall is nonlinear drag,

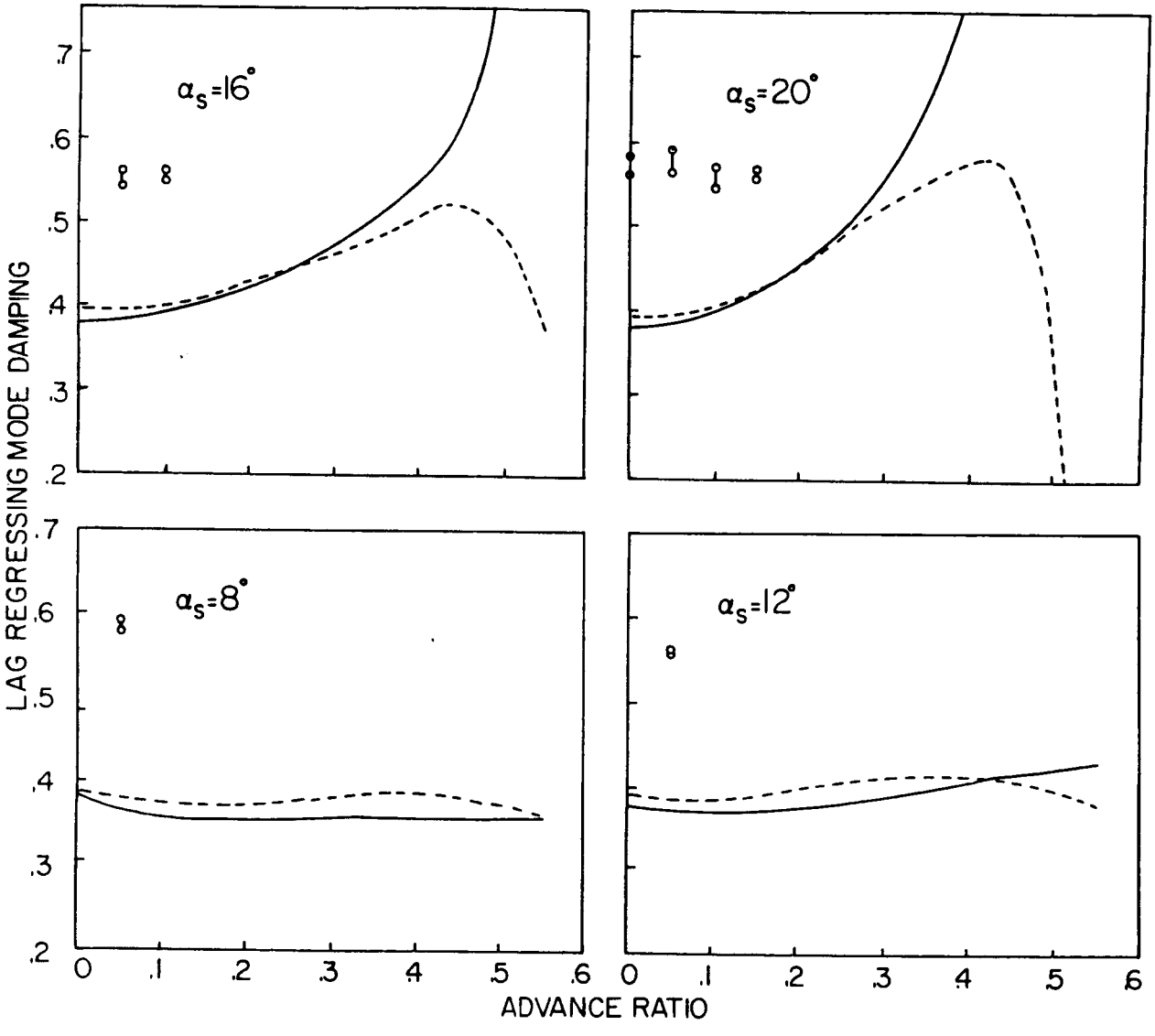

FIG 8 CORRELATION OF LAG REGRESSING MODE DAMPING WITH AND WITHOUT STALL EFFECTS IN FORWARD FLIGHT FOR θ_o=6°

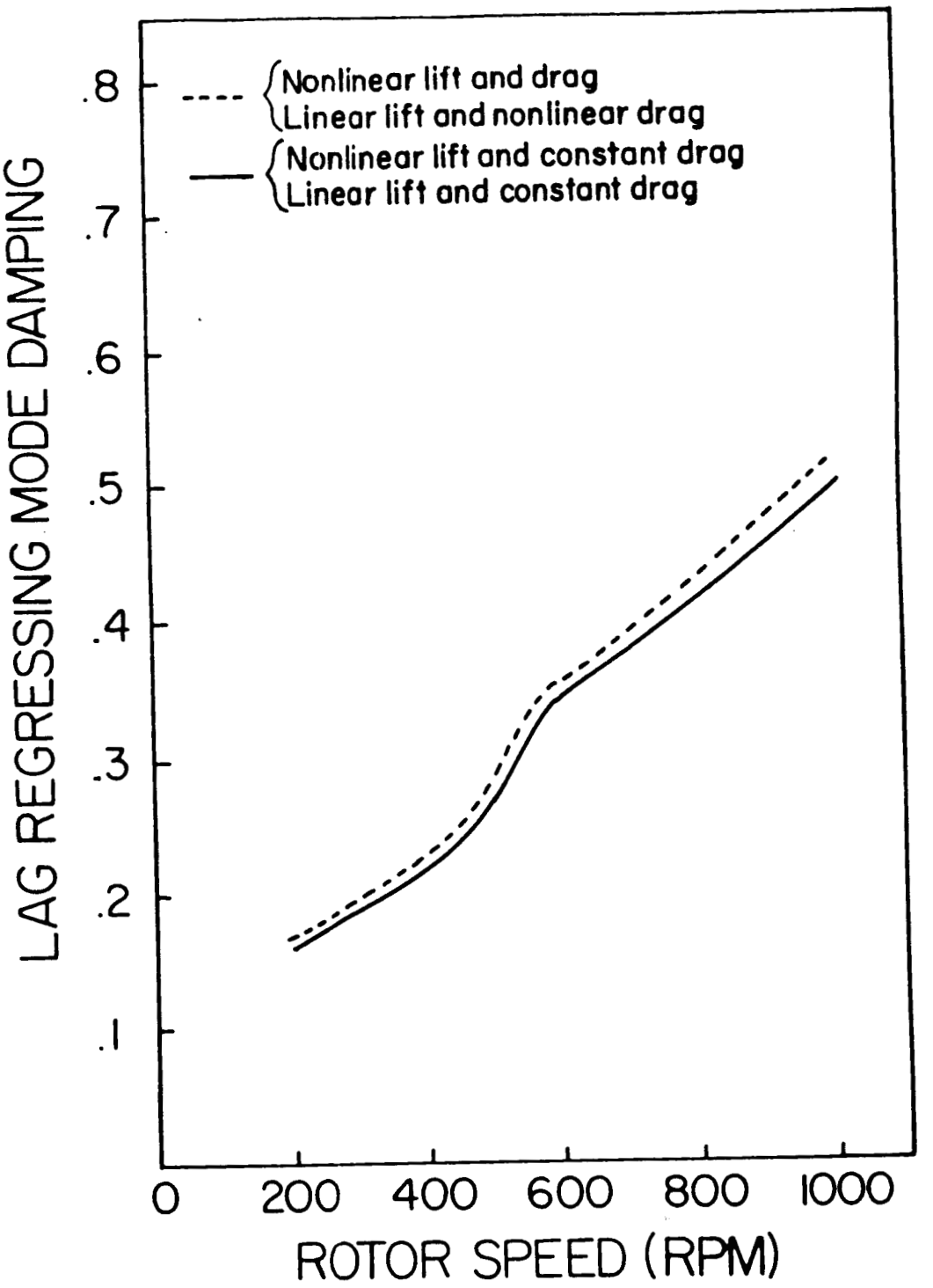

FIG.9 ISOLATION OF THE EFFECTS OF NONLINEAR LIFT AND DRAG IN HOVER FOR $\theta_0 = 8.^\circ$

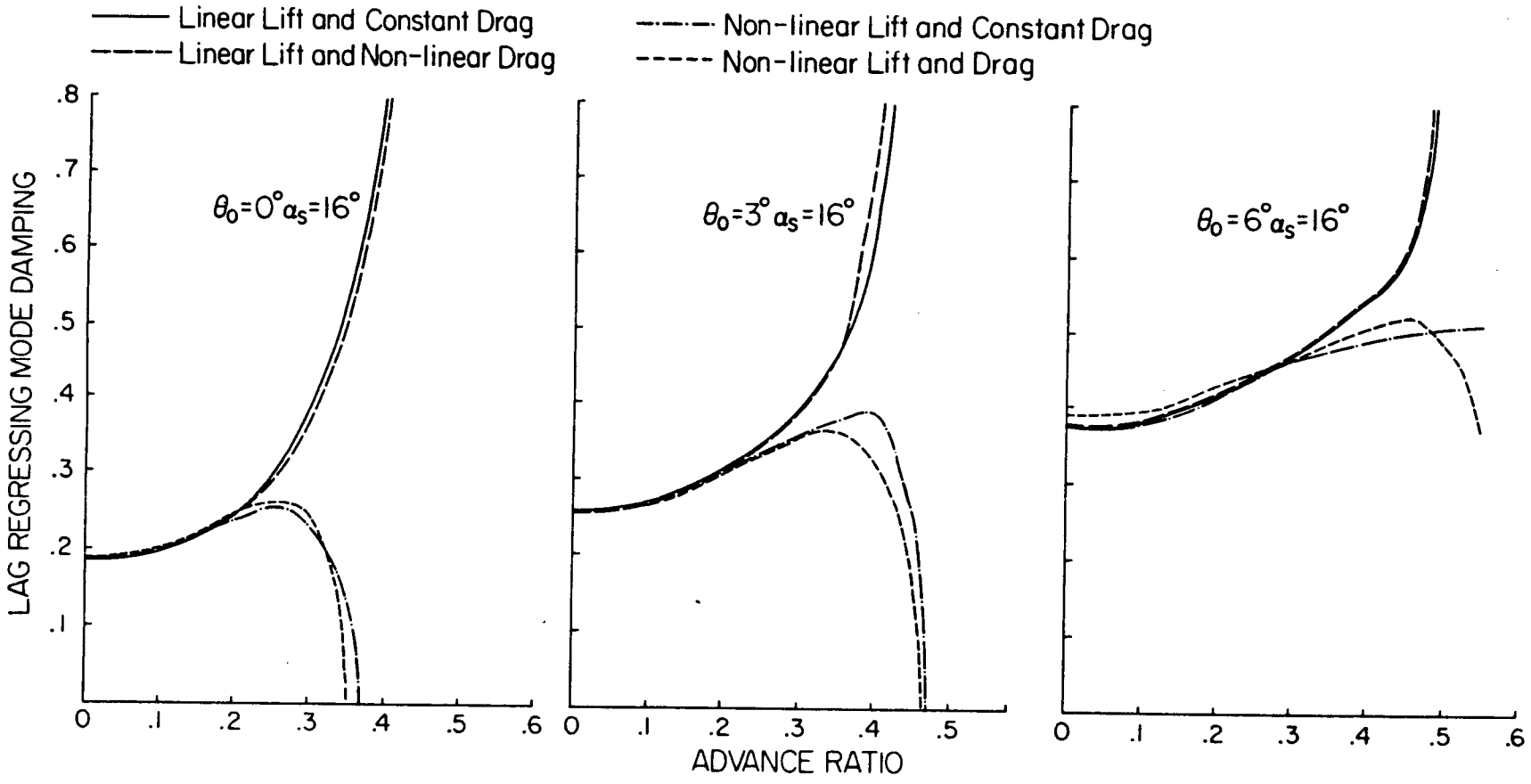

FIG.10 ISOLATION OF THE EFFECTS OF NON-LINEAR LIFT AND DRAG IN FORWARD FLIGHT ($\alpha_s=16°$)

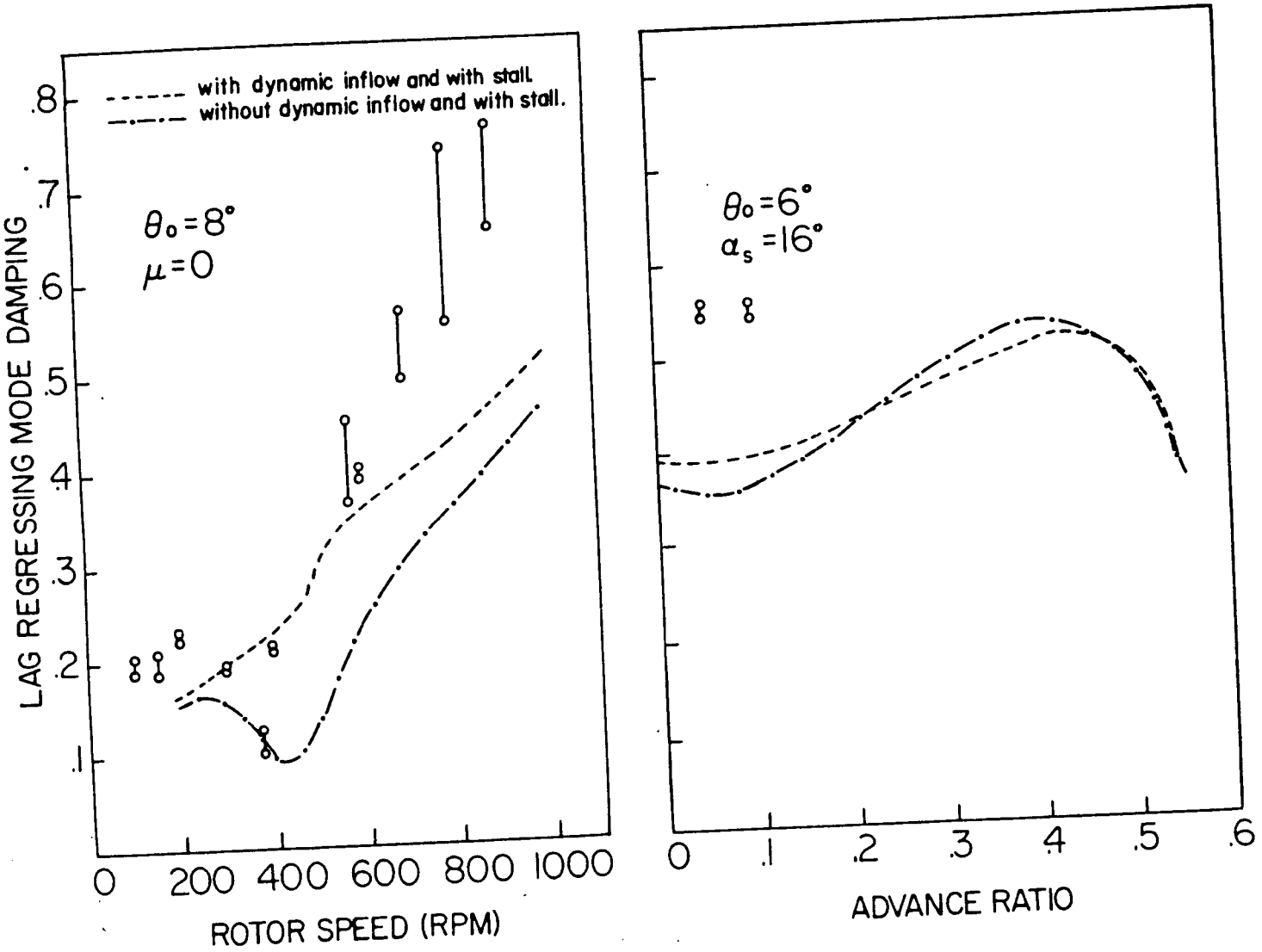

FIG.11 EFFECTS OF DYNAMIC INFLOW ON LAG REGRESSING MODE DAMPING WITH STALL.

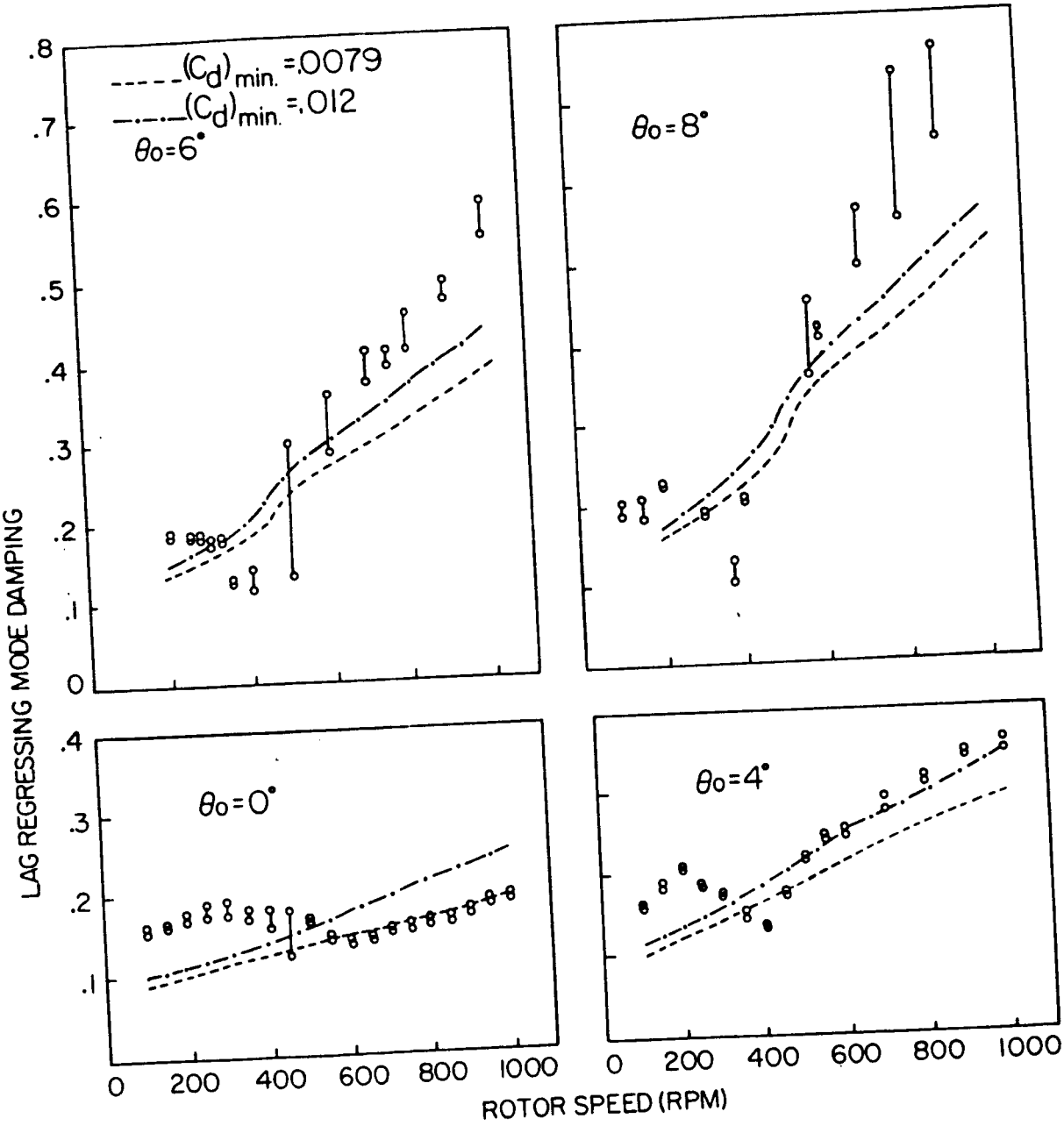

FIG.12 LAG REGRESSING MODE DAMPING WITH $(C_d)_{min}$ = .0079 AND .012 IN HOVER WITH STALL

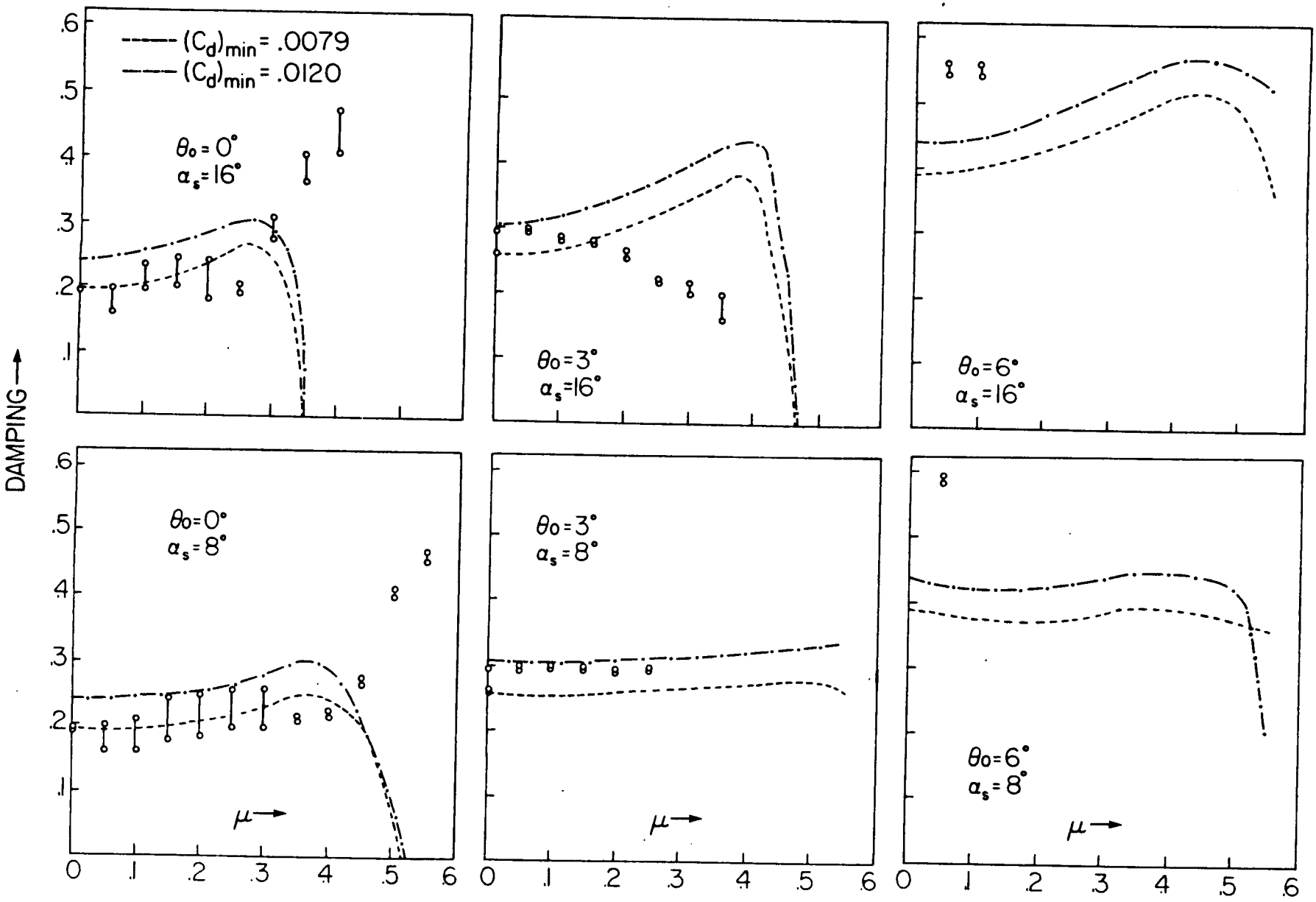

FIG. 13 LAG REGRESSING MODE DAMPING WITH (Cd)min=.0079 AND $(C_d)_{min}$ = .012 IN FORWARD FLIGHT.

although for the specific case in figure 9, its impact is not appreciable. Nevertheless, the simplicity of the hovering case lays the ground work for the more demanding forward-flight case taken up next.

Figure 10 shows the predictions for the same four combinations of lift and drag characteristics treated for the hovering case and these combinations are identified in figure 10. We have included all the three cases with θ_0° = 0, 3, and 6 as treated earlier (figures 4, 6, 7 and 8). In substall, the predictions are as expected. However, when stall becomes an issue, that is, when more than 10-12% of the disk is in stall (θ_0° = 0, $\mu \geq 0.225$, θ_0° = 3, $\mu \geq .225$ and θ_0° = 6, $\mu \geq .3$) the trends of the predictions are extremely interesting, particularly of the predictions from the nonlinear-lift and constant-drag theory. It is seen that the key ingredient is nonlinear lift (and not nonlinear drag) that affects the prediction qualitatively (increasing or decreasing damping with increasing μ).

In figure 11, we address the question of how much better is the stall theory with dynamic inflow when compared to the stall theory without dynamic inflow. In hover dynamic inflow improves the correlation consistently and throughout. In forward flight the impact of dynamic inflow is negligible and a typical example is shown in figure 11 for θ_0° = 6 and α_s° = 16.

Finally, in figures 12 and 13, we discuss the sensitivity of the predictions to the assumed values of c_d (α = 0) or $c_{d,min}$ values. While figure 12 refers to the hovering conditions for four values of the collective pitch setting (as in figure 3), figure 13 refers to the forward flight conditions for a typical cross section of the data in forward flight, as in figures 6,7, and 8. In substall, the higher value .012 gives better overall correlation both in hover and forward flight. This covers all the hovering data and part of the data in forward flight as discussed earlier. When more than 10-12% of the disk is in stall, we know from figure 11 that the predictions are qualitatively affected by nonlinear local lift and not by nonlinear local drag. This is well borne out by the results in figure 13 which shows that the qualitative aspects of the prediction in stall are not sensitive to reasonable changes in the assumed $c_{d,min}$ values.

CONCLUDING REMARKS

1. When less than 10-12 percent of the disk is stalled the linear and non linear theories give nearly the same results, with the nonlinear theory marginally better. When 10-20% of the disk is in stall, the nonlinear theory may

slightly improve the correlation. However only a limited number of data are involved in this range and this improvement is not conclusively demonstrated.

2. For highly stalled cases in forward flight, when more than about 25 percent of the disk is stalled, the stall theory differs markedly from the linear theory, but neither theory does well. However, the linear theory seems to be "qualitatively accurate" for $\theta = 0°$. That the linear theory shows the qualitative accuracy is peculiar since appreciable stall effects should be expected. That the highly stalled, high advance ratio cases are not well predicted by the nonlinear theory perhaps indicates dynamic stall effects.

3. In hover, the data is in substall, and the difference between the stall theory and data increases with increasing Ω and θ_0. This difference is not associated with nonlinear local drag characteristics. The correlations were conducted for $C_{d,min} = 0.0079$ and 0.012. The latter higher value gives better correlation in hover, and in forward flight in substall. Under stall conditions of forward flight, the qualitative aspect of the correlation is not sensitive to perturbations in $C_{d,min}$ values.

4. For stall conditions of forward flight, the key ingredient is nonlinear local lift coefficient which qualitatively changes the prediction when compared with the predictions from the linear theory, and from the theory with linear-lift and nonlinear-drag characteristics. Further, while the theory with nonlinear-lift and constant-drag characteristics is close to the stall theory, the theory with linear-lift and nonlinear-drag characteristics is close to the linear theory.

5. Quasi-steady stall theory with dynamic inflow improves the correlation somewhat in hover but the forward flight results, while qualitatively very different than the linear theory results, do not overall show improved correlation with the data.

ACKNOWLEDGEMENT

We are grateful to Messrs. Robert Ormiston and William Bousman for their encouragement and extensive comments. We also thank Mrs. Sylvia Bone for her hard work and persistence in word processing this paper. This work is sponsored by the U. S. Army Aeroflightdynamics Directorate, NASA-Ames Research Center under grant no. NCC 2-361, and by the U. S. Army Research Office under grant no. DAAL03. The view, opinions and/or findings contained in this report

are those of the authors, and should not be construed as an official Department of the Army position, policy, or decision, unless so designated by other documentation.

REFERENCES

1. Gaonkar, G.H., McNulty, M.J. and Nagabhushanam, J., "An Experimental and Analytical Investigation of Isolated Rotor Flap-Lag Stability in Forward Flight", NAS2-361, U.S. Army Aeroflightdynamics Directorate, July 1986, (11th European Rotorcraft Forum, London, England, September 10-13, 1985, Paper No. 66, Revised).
2. Bousman, W.G. and Ormiston, R.A., "A Study of Stall Induced Flap-Lag Instability of Hingeless Rotors", 29th Annual National Forum of the American Helicopter Society, Washington, D.C., May 1973, Preprint No. 730.
3. Bousman, W.G., Sharpe, D.L. and Ormiston, R.A., "An Experimental Study of Techniques for Increasing the Lead-Lag Damping of Soft Inplane Hingeless Rotors", 32nd Annual National V/STOL Forum of the American Helicopter Society, Washington, D.C., May 1976, Preprint No.1035.
4. Jacobs, E.N. and Sherman Albert, Airfoil Section Characteristics as Affected by Variations of the Reynolds Number, NACA Report No. 586, 1937.
5. Critzos, C.C., Heyson, H.H., and Boswinkle, R.W., Aerodynamic Characteristics of NACA 0012 Airfoil Section at Angles of Attack from 0 to 180, NACA Technical Note No. 3361, 1955.
6. Nagabhushanam, J., Gaonkar, G. H., and Reddy, T. S. R., "Automatic Generation of Equations for Rotor-Body Systems with Dynamic Inflow for A Priori Ordering Schemes", Seventh European Rotorcraft Forum, Garmisch-Partenkirchen, Federal Republic of Germany, September 8-11, 1981, Paper No. 37.
7. Nagabhushanam, J. et al. Users' Manual for Automatic Generation of Equations of Motion and Damping Levels for Some Problems of Rotorcraft Flight Dynamics, R & R Report, HAL-IISC Helicopter Training Program, Indian Institute of Science Bangalore, India, October, 1984.